THESIS

POROUS PROTEIN MICROCRYSTALS AS A SCAFFOLD FOR NUCLEIC ACIDS AND PROTEINS

Submitted by

Mahmoud Masri

Department of Chemical and Biological Engineering

In partial fulfilment of the requirements

For the Degree of Master of Science

Colorado State University

Fort Collins, Colorado

Summer 2022

Master's Committee:

Advisor: Christopher Snow

Christie Peebles
Takamitsu Kato

ABSTRACT

POROUS PROTEIN MICROCRYSTALS AS A SCAFFOLD FOR NUCLEIC ACIDS AND PROTEINS

Oral delivery of nucleic acids is restricted by a number of limiting factors, particularly protection of guest DNA and RNA from degradation and hydrolysis within the gastrointestinal tract following ingestion. Highly ordered, self-assembling porous protein crystals have been previously explored for enzyme immobilization, and may offer similar advantages for protection and targeted delivery of therapeutic molecules to cells. We have developed a reproducible method for generating sub-micrometer porous microcrystals from CJ, a putative isoprenoid-binding protein from *Campylobacter jejuni*, which are non-cytotoxic and capable of passively retaining plasmid DNA and small interfering RNA. Furthermore, we have demonstrated that CJ microcrystals are able to deliver functional plasmid and transfect cells in vitro. In addition to nucleic acids, CJ microcrystals are also capable of adsorbing functional Nanoluciferase, and display chemiluminescent activity following exposure to substrate. The results of this study demonstrate that porous protein microcrystals can serve as a suitable scaffold for RNA, DNA, and functional enzymes, and may represent a viable alternative to spherical nanoparticles and liposomes for therapeutic delivery.

ACKNOWLEDGMENTS

I would like to first thank my advisor, Dr. Christopher Snow for his patience, support, and great suggestions and advice for troubleshooting experiments and for improving my ability to present my work to the group. His enthusiasm for science and his patience has got me to fall in love with what I have worked on and the environment that I was in. I have learned a lot from him, not just the science that I worked on, but also the love for science, being supportive to the people around you, and patience. Also, I would like to thank my mentor, Alec Jones who showed me the ropes around the lab. Taught me many of the methods and techniques that I currently know and used in this project. I would also like to thank Abby Orun, whose expertise in crystallography have helped me greatly with the crystallography projects that I worked on. Also, I would like to thank Julius Stuart in providing advice and suggestions regarding DNA release from crystals. Lauren Beatty for helping me with crystallizing CJ protein and have helped me do qPCR experiments.

TABLE OF CONTENTS

I. BACKGROUND AND MOTIVATION

MOTIVATION

Nucleic acids are macromolecules that are found in all living cells where they serve as the repository for information. Science has progressed to the point where these nucleic acids can also be the basis for nanotechnology where material can be manipulated at the molecular level. Designed DNA structures have been used in various biotechnological, pharmaceutical, and nutritional applications. In 1959, mathematician Albert Hibbs and physicist Richard Feynman proposed the concept of "swallowing the surgeon" where tiny robots enter the interior of the body to identify the problem and repair it (6). R. Feynman, a professor at California Institute of Technology, delivered a lecture called "There is a lot of room at the bottom" where the possibility of building molecular structures was promoted (38). Following that lecture, the term "nanotechnology" was not used until 1974, by Norio Tanaguchi at an international conference about manipulating a single nanoscale object. This futuristic vision for the medical field was credited to Hibbs and his concept of "swallowing the surgeon" (6). In recent decades, these early ideas have become a reality where biomolecular engineering and nanotechnology come together as "Nanobiotechnology". Nanotechnology use in medical fields has grown significantly in the past few decades for biomarkers, molecular diagnostics, drug discovery, and drug delivery (11). In particular, nanomedicine is significantly growing to improve quality of life by treating diseases such as cancer and for faster diagnostic methods. Many nanotechnologies are used in the medical field where drug delivery is an essential part of modern medicine. Nanosized molecular assemblies are capable of carrying therapeutic drugs, DNA/RNA, or proteins (9). Delivery to the desired targets through biological barriers is important for optimizing the

therapeutic load (18). Nucleic – acid – based therapeutics targeting the genetic bases of various diseases for treatment or cure are getting approved by various international counterparts to the Department of Health and Human Services in the U.S. A nucleic acid (NA) payload might counteract defective genes to achieve therapeutic effect; however, one of the challenges that comes with the use of nucleic acids for therapy is that they are prone to degradation by nucleases (21). The ideal delivery platform should be able to provide such protection to the nucleic acids from various environmental challenges. Through computational methods and protein engineering, we have reached the potential to manipulate molecular interactions to develop next – generation inventions such as drug delivery vehicles which encapsulate therapeutic drugs and deliver them to target locations while protecting the drugs from surrounding harsh environments (37).

The 2 most common types of nucleic acids are RNA and DNA, and both are formed from nucleotides that contain a five – carbon sugar backbone, phosphate group, and a nitrogen base, however, DNA contains thymine while RNA has uracil nucleobase. Additionally, RNA contains the sugar ribose while DNA has deoxyribose (deoxyribose sugar lacks an oxygen atom). This chemical difference makes RNA prone to hydrolysis, and therefore less stable than DNA. Protection from hydrolysis is important when delivering RNA for therapeutic purposes. It is well-known that RNA is involved in various medical applications such as diagnosis, therapy, and vaccines such as Moderna and Pfizer SARS-COVID-19 vaccines. Vaccine platforms of interest involve: viral vector-, protein-, RNA-, and DNA – based vaccines in which the process of developing the vaccine includes developing a delivery method (32). Lipid – based nanoparticles

(NP) are a well-known example. Here, we evaluate protein crystals as an alternative potential carrier that could adsorb and provide protection to NA guests.

Using protein crystals as a delivery vehicle for nucleic acids could result in a decrease in their rate of nucleic acid hydrolysis. The first protein crystal was reported in 1840, made of hemoglobin (39). Since then, nano – scale protein crystals have been used in drug delivery (39). Protein crystals structures that consist of protein molecules, water, and other chemical molecules (small molecules, ions, etc.) are typically fragile due to their weak mechanical properties (39, 42); they break or degrade quickly if they are not sustained in a stabilizing solution. Protein crystals are held together by relatively weak intermolecular interactions (hydrophobic interactions, H-bonds, etc.) (19). Thus, biomolecular crystals are weaker and easier to break than non-biological crystals (19). Thanks to rapid development of the field of protein crystal engineering, crystal fragility can be readily resolved by crosslinking (36). Therefore, after crystallizing the protein and before loading it with the therapeutic agent, most crystals will need to be crosslinked to make them tougher and able to protect guest agents. Crosslinked protein crystals are more able to withstand solutions with different salt concentrations (11).

Crosslinking is the addition of a chemical interaction in the form of strong intramolecular bonds between protein molecules forming a more robust structure (42). Introducing covalent bonds between adjacent monomers has been shown to greatly improve crystal stability, which expands the potential application uses for protein crystals (12).

In addition to RNA, proteins are another potential therapeutic payload. Over 500 biopharmaceuticals have either been approved or are in advanced clinical trials (3). Protein

crystals could again be an advantageous delivery platform if the crystal lattice is sufficiently porous to allow guest protein adsorption. The payload would be resistant to degradation if the host crystal lattice were to act as a shield against proteinases, and other factors that contribute to degradation.

Crystals also provide advantages of better handling and stability (19). Additionally, the use of crosslinked protein crystals for delivery of vaccines could increase shelf stability, enable extended release, and/or solve problems related to immunogenicity by slowly releasing drugs. The highly repetitive structure of epitopes in protein crystals could provide enhanced immunogenicity per a study performed by N. St. Clair, et al (36).

Protein crystals are the end product of highly ordered protein self – assembly. We have previously produced nanoporous protein crystals from a putative polyisoprenoid – binding protein from *Campylobacter jejeuni* (CJ) (20). This study focuses on evaluating these "CJ" crystals as a nucleic acid delivery chassis. In this thesis, methods were first optimized to grow CJ nano – sized crystals. Second, methods were developed to assess the extent of protection provided to adsorbed nucleic acids by CJ protein crystals using a combination of developed qualitative and quantitative assays. Third, methods were designed to measure the rate of release of loaded guest nucleic acid as a function of ATP concentration.

The ultimate goal of hosting RNA within protein crystals is to advance the oral delivery of RNA to mammals. This hypothetical technology would capitalize on the extraordinary promise of RNA as a therapeutic agent. The key question is whether porous host protein crystals

can compensate for the intrinsic susceptibility to degradation of the guest RNA and would serve as a capable delivery device with the ability to confer stability and protection. To achieve this goal, we first grew protein nanocrystals in batch settings and were able to reproduce nanoscale protein crystals smaller than 300 nm. Second, we demonstrated that the protein crystals can adsorb and retain RNA, DNA, and protein. In addition, following adsorption of guest NA, we demonstrated that the host crystal would be stable while being exposed to nucleases using a confocal microscope to quantify the integrity of the guest DNA or RNA. Lastly, using continuous flow in a microfluidic device, we imaged the guest protein crystal adsorbing fluorescent labeled DNA and measured the rate of release in different ATP concentrations. ATP is a potential release factor for triggered cargo release.

BACKGROUND

RNA Used in Gene Therapy

Drug development based on the use of either nucleic acids or proteins has the potential to treat and cure patients. There are treatment strategies that attempt to permanently alter a patient's DNA, also called gene therapy and have been pursued to treat genetic disorders and combat cancer. There are tremendous benefits for the use of RNA therapy compared to gene therapy. First, messenger RNA (mRNA) has no viral promoters or bacterial sequences which could lead to toxicity. Second, mRNA does not integrate into the host genome. Third, mRNA is safer because gene expression through mRNA is transient compared to DNA. Lastly, mRNA need not pass through the nuclear envelope, which increases the chance of transfecting cells successfully (31). Research has made significant progress in the past few decades on developing nucleic acids-based therapeutics (35). For example, small interfering RNA (siRNA) have demonstrated

use for the treatment of fatal diseases or diseases that have limited treatment options (15, 24). mRNA has also been emerging as a new class of nucleic acid therapeutics that is used in gene therapy (31). Nucleic acid therapies to treat various genetic diseases have evolved from tools such as transcriptor activator – like nucleases (TALENS), RNA silencing, and clustered regularly interspersed palindromic repeats (CRISPER). Scientists are using these tools to reveal the genetic basis of various diseases such as cancer and type 2 diabetes (22). Arguably one of the most promising and high-profile use cases is DNA/RNA based vaccines (22). During the SARS – CoV – 2 pandemic, mRNA vaccines were developed by Moderna and Pfizer to protect against infectious diseases such as COVID – 19. These vaccines function by causing our cells to produce the SARS – CoV – 2 spike protein. Generally, many vaccines were developed using various platforms such as RNA (by Moderna and Pfizer) and DNA (by Vaccine Institute and Symvivo) when the pandemic hit around 2020, that would deliver genetic materials encoding antigen candidate into the host cell using lipid nanoparticles as a delivery platform (32). Because of the instability of the naked mRNA and DNA, mRNA and DNA based vaccines require the use of delivery vehicles especially since the mRNA and DNA would have to pass through harsh environments to reach their target (32). However, lipid nanoparticles are not stable enough to allow oral delivery.

RNA interference (RNAi) could also neutralize target mRNA to inhibit gene expressions and thereby treat diseases. Specifically, RNAs with sequence complementarity to a gene's coding sequence can lead to mRNA degradation which then prevents the translation process of mRNA to protein. RNAi functions by integrating one of the strands of the duplex small interfering RNAs (siRNAs) and turn it into a mRNA – targeting effector complex, also known as

RNA – induced silencing complex (RISC) (15). siRNA is typically used for transient gene silencing (15). Multiple disease targets have been knocked down *in vivo* using synthetic (siRNA). The generality of the siRNA approach leads to great potential when fighting diseases such as cancer or viral infections. Where abnormal expression or mutation occurs, siRNA is incredibly attractive because it could function in the cytoplasm and does not require nuclear penetration (35). siRNA strands typically do not exceed 25 nucleotides in length which is synthetically accessible making them easily designed and developed (35).

Challenges Working With RNA

Although RNA offers great benefits for the purpose of therapeutics and various other applications, RNA structural and sample integrity are critical challenges to address. Compared to DNA, the presence of the 2' hydroxyl group renders RNA more prone to hydrolysis. RNA is therefore less stable than DNA at room temperature. For therapeutic uses, the integrity of the RNA must be maintained throughout the entire process. Sample integrity is also hard to maintain while working with RNA because of RNase contamination. RNase is ubiquitous; it can be found on or in human tears, skin, blood, sweat, and saliva. Without the proper usage of aseptic techniques, it is hard to keep RNA strands intact. The rate at which some RNase enzymes degrade RNA is around 39.2 nmol/min per mg (1). Oxidation could also result in RNA degradation through regular atmospheric pollutants that react significantly with RNA. Pollutants are not required but do accelerate the process. Another method for degradation to occur is through the activity of metallic complexes catalyzing the hydrolytic cleavage of the phosphodiester bond (4). RNA is typically held at -80 °C for long term storage and -20 °C for short term storage to reduce degradation. However, it has been shown that some ribonucleases

maintain activity at -20 °C (4). Therefore, aliquoting RNA samples for single use to avoid thawing – freezing can help reduce degradation. In addition, RNA is very sensitive to pH. Altogether, working efficiently in a clean RNase-free environment while avoiding unnecessary thawing-freezing steps is vital to ensure RNA integrity.

CJ Protein Crystals as Delivery Device

While most biomolecular crystals can adsorb small molecules, porous crystals have the ability to uptake guest *macromolecules*, which allows various applications involving drug delivery and biosensing (13). It was shown that CJ protein crystals have the ability to adsorb and retain nucleic acids (17) and enzymes (20). As shown by Wang et al. CJ protein crystals have the ability to adsorb and retain nucleic acids. The unusually large pores give CJ crystals the capacity to uptake dsDNA (40). CJ crystals are highly porous, with ~13 nm – diameter nanopores arranged hexagonally, resembling the structure of a honeycomb when observed using high resolution atomic force microscopy (AFM) (Fig. 1). Coaxing the protein to crystallize to the right size and crosslinking it to make it stable are not trivial challenges due to the difficulty of precisely controlling nucleation and growth phenomena. Nonetheless, CJ crystal size is tunable in the lab, and we can achieve crystals small enough (~300 nm) to theoretically enable delivery in the blood stream of the human body (37). In addition, crystal stability can be dramatically improved with chemical crosslinking, which will also be important for use in the blood stream. Enzyme adsorption and retention in the pores of CJ protein crystals provided long term enzyme stability and increased thermal tolerance (20); motivating possible uses as sensory and delivery devices (20). Protein crystals are also an attractive scaffold from a biodegradability and/or biocompatibility standpoint. Protein crystals have been used successfully in pharmaceuticals

(drug delivery, vaccinations, biosensing, etc) for decades due to their favorable handling, stability, and tunable payload release properties (12, 2). For example, in 1930s, protein crystals were developed to deliver insulin which kickstarted the development of microcrystalline structures known as NPH insulin (2). Crystalline insulin was the first therapeutic crystalline protein to get approved for use (3). Crystals are also attractive because of ease of scaling production and dose release control based on size and shape (36, 13). In addition, the usage of crystals to deliver small therapeutic agents as a form of treatment have shown various advantages that include significant chemical degradation reduction in crystal structures unlike many competing carrier biomaterials (19). Among all drug delivery materials, crystals are unusually scale invariant in the sense that the nanostructure is the same for tiny or large crystals compared to soluble form or amorphous (19).

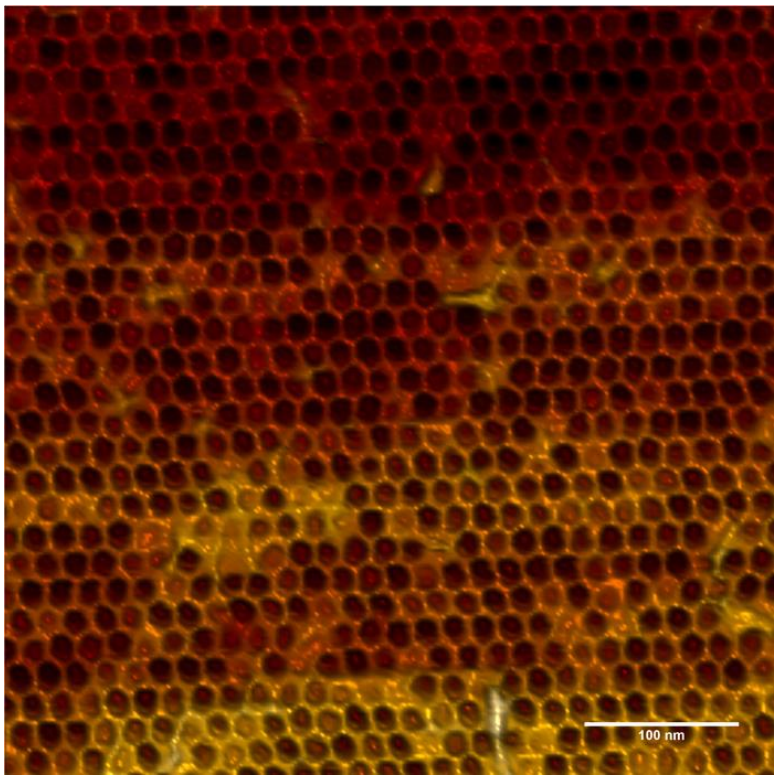

Figure (1): Image of the CJ pores taken using the AFM by Wang, et. al. 2021

The process of making protein crystals involves an ultra-pure protein sample and concentrated precipitant (3 – 3.3 M ammonium sulfate for CJ). There are 3 different methods that are widely used: sitting and hanging drop vapor diffusion, and batch crystallization. The methods used here were sitting drop vapor diffusion and batch crystallization. Sitting drop experiments contain a reservoir solution composed of varying concentrations of salt, buffer, and precipitant. The mixture is then pipetted into the middle podium that contains the protein sample. Sitting drop experiments were used to grow large crystals that are over 80 µm in diameter. On the other hand, batch crystallization was used for increased production of smaller crystals, typically microcrystals, but as small as (~300 nm). Previous crosslinking protocols used in the Snow lab used 100 – 500 µm CJ crystals washed in a high salt buffer followed by crosslinking with one of 3 potential alternative chemical agents: 1-Ethyl-3-(3-(dimethylamino)propyl)- carbodiimide (EDC), glutaraldehyde (GA), or oxaldehyde (OA) mixed with high salt buffer, and para-Dimethylaminobenzaldehyde (DMAB) and allowing the crystals to crosslink sometime between 1:30 – 2 hours. After crosslinking, crystals were looped to one of the following quenching solutions hydroxylamine or borate for about the same length of time as the crosslink; after the quench finishes, the crystals were washed again then placed in a storing solution (12). CJ protein crystals of 80 µm size or CJ nanocrystals were both crosslinked with 1% glyoxal followed with 1 M hydroxylamine quench pH 6. Both large crystals and nanocrystals were used to host RNA in varying pH and with the presence of RNases to quantify the extent of protection provided by the host crystals.

Methods to Quantify and Assess RNA Integrity

Assessing RNA integrity is a crucial aspect in research and manufacturing of RNA based pharmaceuticals and biotechnology. Since RNA is sensitive and prone to degradation, various tests must be performed to ensure non-degraded RNA. One of the most frequent methods used to determine nucleic acid quality is denaturing gel electrophoresis. It is important to be able to determine the precise size of RNA, and there have been major improvements since the 1970s in electrophoretic techniques using purified agarose or polyacrylamide (28). The benefits of using a classic TAE agarose gel for RNA size determination are simplicity, speed, and affordability. For proper analysis, RNA samples are prepped with hot formamide which disrupts RNA secondary structure (1). By denaturing the RNA, RNA secondary structure is suppressed ensuring that the final position in the gel is correlated with RNA length (34).

Another popular method of quantifying nucleic acids is using quantitative polymerase chain reaction (qPCR). PCR was a foundational invention in molecular biology and is widely used in various applications including mapping genomic sequences. PCR is also the gold standard method to detect bacterial and viral infections such as COVID-19 (by amplifying viral genomic sequences). PCR is a relatively quick process where the results are received within a few hours and is conveniently performed in a laboratory thermocycler. PCR works by first denaturing the DNA at ~95 °C, separating the DNA strands at a slightly lower temperature (60 °C) from each other and producing two single strands instead of one double stranded DNA where the DNA primers attach to each template DNA. The temperature is then raised (72 °C), and the new strand of DNA is made by a polymerase enzyme (e.g., Taq polymerase) generating complementary strands hybridized to each of the original strands. Repetition of the denaturing,

annealing, and elongation steps leads to exponential strand duplication. Many repetitions (30 - 40) result in billions of DNA strand copies.

Since the PCR protocol was invented, numerous variations have been devised (e.g., RT-PCR, qPCR, and RT-qPCR). Reverse transcriptase PCR (RT-PCR) works primarily with RNA, using reverse transcription to convert RNA to DNA prior to PCR amplification. For the purpose of detection, it is recommended to use qPCR which relies on fluorescence to quantify the growing DNA population. With RNA being prone to high risk of degradation, RT-qPCR is the best way to be able to quantify and detect RNA and be able to assess its integrity.

We used multiple methods to quantify how well CJ crystals retain and protect RNA from various environmental conditions. First, a TAE agarose denaturing electrophoresis gel was used to test the size of the RNA after RNase A challenge, with and without adsorption to CJ crystals. Second, we developed a quantitative RT - qPCR assay per a study performed by Padhi et al. to quantify the amount of full-length intact RNA remaining (after elution from host crystals) by comparing two amplicons (Fig. 2). Specifically, we measured the relative expression of two amplicons derived from the 3' and 5' ends of the RNA strand. This assay relies on the directionality of the reverse transcription reaction, which always proceeds from the 3' end of the RNA strand to the 5' end, synthesizing a cDNA strand from the 5' to the 3' direction (23). In theory, if the RNA is intact, the reverse transcription reaction should proceed to completion, generating full length DNA and therefore leading to a ~1:1 ratio of 3' and 5' amplicons. In case of significant degradation, reverse transcription will yield numerous partial DNA sequences that

do not extend to the 5’ amplicon region. In this case, the 5’ amplicon would be lower which would result in a higher 3’:5’ ratio (30).

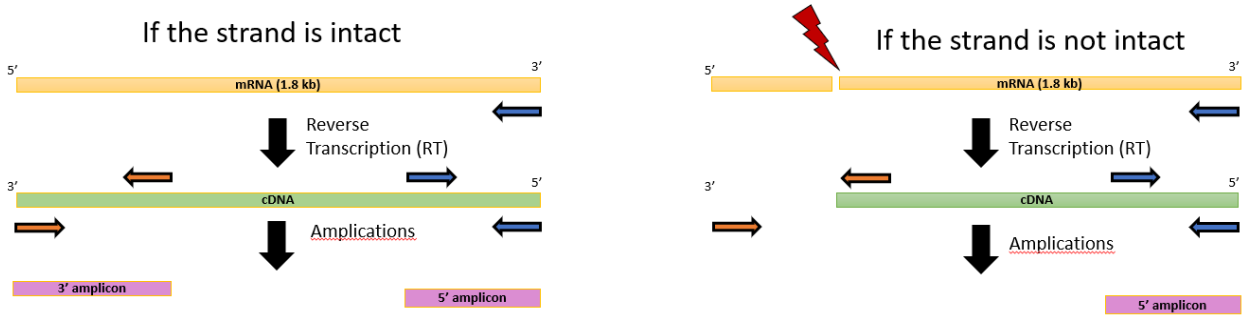

Figure (2): Illustration of quantifying the number of full-length intact RNA using RT-qPCR

Another quantitative assay was based on Fluorescence Resonance Energy Transfer (FRET) with a 35 mer DNA probe that contained a 5’ – terminal FAM (green) and a 3’ – terminal TAMRA (red) FRET pair (Fig. 3). A description of FRET probe design and application was written by Didenko., V., where a DNA probe of 2 fluorophores within 10 nm of each other can transfer energy at an efficient rate (8). The idea is that a nucleic acid sequence would contain 2 fluorophores such that one fluorophore donates excitation to an acceptor fluorophore. A dipole – dipole interaction causes the acceptor molecule to excite while the donor is quenched. If the probe oligonucleotide is hydrolyzed, the intensity of the donor molecule would increase over time in exchange to a decrease in the intensity of the acceptor molecule (8).

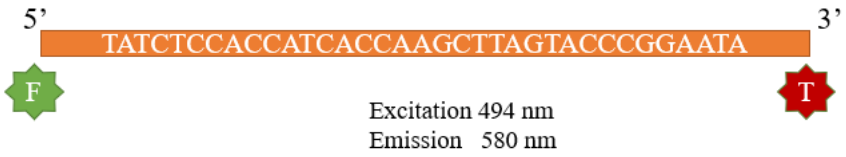

Figure (3): FRET – based ssDNA probe

Microfluidic Devices

Microfluidic devices are an increasingly popular strategy for automating and miniaturizing chemistry and biology experiments. The devices tend to consist of channels, chips, sensors, and various other features on the μm to mm scale. The devices provide great benefits of speedy data analysis and significant reduction in reagent volume by integrating multiple components in one device (26). In addition, the devices can be built for laminar mixing flow. Such devices could be used for detection and diagnosis where they offer the ability to separate molecules and to detect various analytes and antibodies with great sensitivity (29). Often these devices can be designed and constructed using simple and affordable materials, enabling production of diagnostic devices at low cost. By integrating the components needed for sample processing, fluid handling, signal amplification, and detection in one device without the need for electricity or moving parts, rapid onsite diagnosis could be performed, enabling a higher rate of treatments and health improvements for people in developing countries or natural disaster locations (5). My coworkers and I developed a device to load and release guest nucleic acid into host protein crystals. We were able to measure the release rate of fluorescent labeled nucleic acid by measuring the fluorescence emission intensity of the crystal over time.

In this paper, we demonstrate the capacity of CJ nanocrystals to adsorb, retain, and release of guest NA under similar conditions mentioned earlier. The rate of release of NA from CJ crystals remains unclear. Therefore, microfluidic flow cells were designed and constructed (Fig. 4) to measure the rate of release of guest NA from CJ crystals. The key design criteria is the ability to maintain a continuous fluid flow to visualize loading and release in real time. Adenosine triphosphate (ATP) is a multifunctional nucleotide which consists of phosphate

groups, adenine, and the sugar ribose; because of its structure, it provides energy to the cell through breaking the phosphoanhydride bond (14). ATP also plays an important role in cell functions, membrane transport and degradation of cellular compounds which makes the development of controlled release that is responsive to ATP significant (14). Also, it was shown in previous studies that ATP can release encapsulated cargoes and it is of high interest due to over expressed ATP in certain diseases such as cancer cells and thus, ATP release of drugs could be of great advantage (25). By continuously flowing fluorescently labeled NA, we observed the CJ protein crystal adsorbing guest NA in real time. We hypothesize that ATP will compete with guest DNA for binding sites inside the CJ crystals. To test this hypothesis, we introduced precise concentrations of ATP, observed release of NA in real time, and measured the rate of release as a function of ATP concentration.

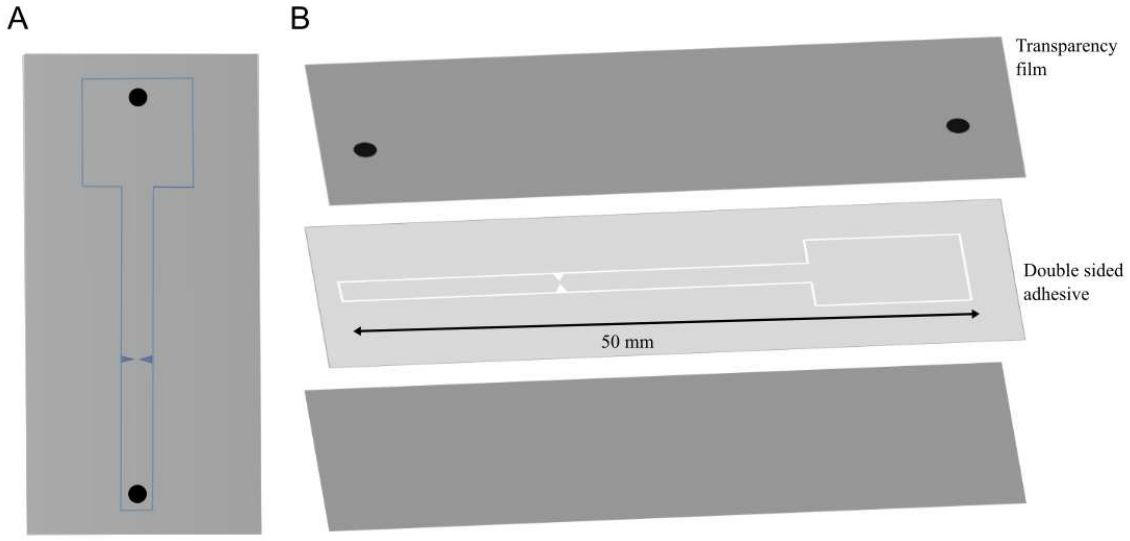

Figure (4): Multi – layered microfluidic device made of transparency layers and double - sided adhesive

III. METHODS

CJ Protein Expression

For the protein expression, Terrific Broth (TB) was prepared by combining 100 mL Phosphate buffer salt, 24 g yeast, 4 mL glycerol, and 20 g tryptophan and brought up to 1 L volume using reverse osmosis (RO) water in 2 L flasks. After mixing using shakers at 250 revolutions per minute (RPM) for about 20-30 minutes, the flasks were sterilized in an autoclave (STERIS Amsco lv 250). After the sterilization, the media was allowed to sit at room temperature to cool to around 50 – 55°C before the addition of antibiotics (kanamycin, 50 µg/mL final concentration). A starter culture was prepared by inoculating 10 mL TB media (with kanamycin) from a glycerol stock containing BL21 gold cells previously transformed with the desired plasmid, and incubated at 37°C, 250 RPM overnight. The culture media was transferred to 2 L flasks (10 mL of culture per 1 L of media) and was allowed to incubate at 37°C, 250 RPM. A 1 mL sample was collected every hour to measure optical density (O.D.) using a NanoDrop One Microvolume UV-Vis Spectrophotometer (Thermo Fisher Scientific) to determine when the liquid culture has reached its optimum exponential phase. After reaching the exponential growth phase (Fig. 5) (41), we induced protein expression, ideally before hitting the stationary phase.

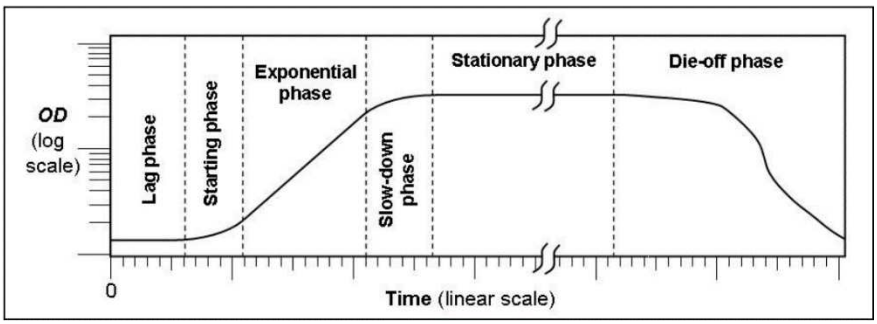

Figure (5): Phases for a bacterial culture (41)

Specifically, protein expression was induced once the cultures reached an OD between 0.7 and 0.85 using isopropyl β-D-1-thiogalactopyranoside (IPTG), an allolactose mimic, at a concentration of 0.4 mM. This was the induction method selected as all plasmids were designed to include a lac operon controlling expression of the desired protein. Following induction, the cultures were incubated at 25°C, 250 rpm for at least 16 hours. Following protein expression, the cultures were transferred to 1 L cylindrical containers and then centrifuged for 20 minutes at 10,000 relative centrifugal force (RCF) to pellet the cell mass. The pellets were weighed by difference and recorded. Following centrifugation, the cell pellet was resuspended in 80 mL of lysis buffer (50 mM HEPES, 500 mM NaCl, 20 mM imidazole, 10% glycerol, pH 7.4) per liter of culture (~4 mL / 1 g of cell paste). The resuspended pellet was transferred to a glass beaker and was allowed to sit on ice water and cool for about 5 – 10 minutes. The resuspended cells were sonicated at 50% power for 10 seconds "ON" / 30 seconds "OFF" (10-minute process time) while on ice water. After sonication, the lysate was transferred to a 50 mL conical tube and centrifuged at 10,000 g, 4°C, 20 minutes twice or until clarified. The lysate was then run on a Ni – NTA (Nickel – nitrilotriacetic acid) metal affinity column, which is designed to purify His-tagged recombinant proteins. The nickel ions on the column resin binds to proteins containing poly-histidine tags, which allows the protein to be bound, washed, and later eluted with elution

buffer (50 mM HEPES, 500 mM NaCl, 10% glycerol, 500 mM imidazole, pH 7.4) which outcompetes the nickel-histidine interactions, allowing the protein to come off the column.

$5'$ *MET HIS HIS HIS HIS HIS HIS XXX XXX XXX* … $3'$

Start codon	CAT/CAC	protein specific sequence
	Histidine codon	

OR:

$5'$ *XXX XXX XXX … HIS HIS HIS HIS HIS HIS TGA* $3'$

protein specific sequence	CAT/CAC	STOP codon
	Histidine codon	

For the column, the clarified lysate was passed over the resin in a 50 mL glass column and allowed to drip slowly through the resin. Following loading (Fig. 6), the resin was washed three times with lysis buffer. After washing, elution buffer was applied to the column and collected in three fractions. "Elution #1" would contain mixture of elution buffer and lysis buffer while "Elution #3" contains whatever left of protein in the column after the second elution. Synthesis of CJ nanocrystals requires extremely pure protein: therefore, the quantity of the yield must be sacrificed for higher purity. Accordingly, the second of the elution fractions was dialyzed overnight into storage buffer (10 mM HEPES, 500 mM $(NH_4)_2SO_4$, 10% glycerol, pH 7.4) using snakeskin dialysis tubing (10k MWCO). After the dialysis, the dialyzed CJ protein was transferred into a 50 mL conical tube and was purified further via ammonium sulfate

precipitation; briefly, three volumes of 4 M ammonium sulfate were added to the dialyzed protein and incubated with gentle rocking at room temperature for 30 minutes. The sample was then centrifuged at 10,000 g for 15 mins at 25°C, and the clarified sample was filtered through a 0.2 µm cup filter. The protein was then concentrated and desalted with Ultra-15 amicon (Merck Millipore #R1JB06172) filters, then diluted with an AS buffer to a final concentration of at least 15 mg/mL. The concentration of the protein was measured via the Coomassie Plus Protein assay (Thermo Scientific #QI221752) using a microplate reader (BioTek Epoch). The protein was subsequently aliquoted and stored at -80°C.

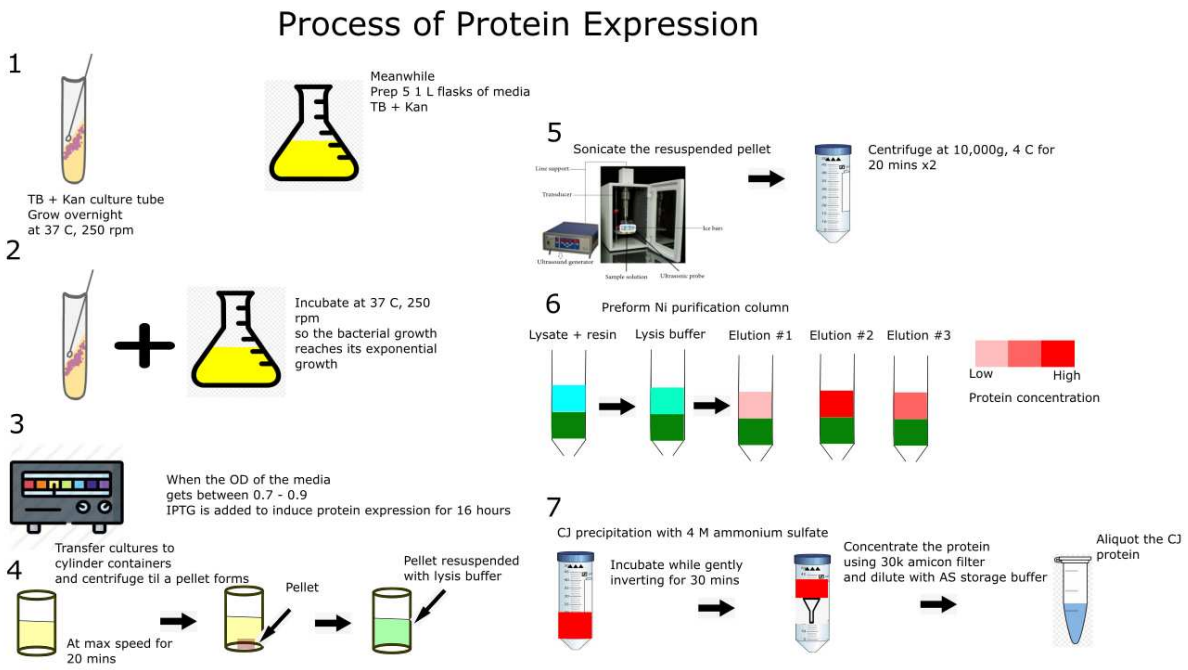

Figure (6): Process of protein expression

Protein Crystallization

Crystals were synthesized using both sitting drop vapor diffusion and batch methods. The components required to perform crystallization are precipitant, buffer, and protein. The sitting drop vapor diffusion was performed in 24 well plates and 96 well plates. The mixing process was done using a Gryphon, an automated crystallization robot, to screen conditions for crystal size optimization. The precipitant salt used was ammonium sulfate, with a concentration ranging from 2.5 to 3.6 M. The buffer was 0.1 M Bis-Tris, with a pH range of 6.5 – 7.5. Precipitant buffer and WT CJ protein (50 mg/mL) were combined with ratios ranging from 25/75 to 50/50% (protein/buffer) in a total volume of 2 µL, and after sealing the wells, plates were incubated at room temperature for at least 24 hours. We adjusted the conditions to optimize crystal sizes; crystallization of narrower conditions aiming for the desired size was achieved on a 24 well plate with precipitant salt concentration ranging from 3.2 to 3.5 M.

In addition to using the sitting drop vapor diffusion method, we used batch crystallization to produce greater quantities of microcrystals, or even nanocrystals as small as (~300 nm). A precipitation buffer consisting of 3.3 M ammonium sulfate, 100 mM Bis – Tris, pH 6.5, and 2.4% PEG 6000 was prepared, vortexe, and then filter sterilized. Five volumes of precipitation buffer were mixed with 1 volume of concentrated WT CJ protein (30-35 mg/mL), to a final volume of 240 µL. The sample was then incubated on a rocker at 4°C for 24 hours.

Crystals grown using both methods were chemically crosslinked using glyoxal. Sufficiently large crystals (>30 µm) that grew in the crystal plates were looped and washed 3

times with 4.2 M TMAO (pH 7.5), then transferred to a crosslinking solution containing 875 µL 4.2 M TMAO (pH 7.5), 100 µL 250 mM DMAB, and 25 µL 40% glyoxal for 30 minutes to 2 hours, depending on the size of the crystals. After the crosslink, the crystals were looped to a quenching solution (1 M hydroxylamine, 100 mM DMAB, pH 6) for a similar length of time. After quenching, the crystals were looped and washed 3 more times with water and stored short-term at 4°C.

The microcrystals were pelleted by centrifugation (2,600 g for 3:00 min). After removing the supernatant, the crystal pellets were resuspended in 4.2 M trimethylamine-N-oxide (TMAO), pH 7.5 by light vortexing. Crystals were allowed to soak for 5 minutes, then centrifuged and resuspended in fresh TMAO. These washes were repeated at least two times. After washing, the crystals were resuspended in a crosslinking buffer (4 M TMAO, 25 mM p-dimethylaminobenaldehyde (DMAB), 1% glyoxal), and incubated on a rotator at room temperature for 1 hour. The crystals were then quenched in 1 M hydroxylamine, pH 5.0, with 100 mM DMAB, for 30 minutes. Following quenching, the crystals were resuspended in a microcrystal storage buffer (50 mM HEPES, 10% glycerol, pH 7.5) and stored at 4°C long-term.

Size and concentration determination of CJ microcrystals

Scanning electron microscopy (SEM) was performed on a JEOL 6500 scanning electron microscope. Crystals were deposited on an aluminum substrate and dried under vacuum, gold sputtered to 10 nm thickness, and imaged with 15 kV beam. Dynamic light scattering (DLS) and zeta potential were measured using a Zetasizer Nano ZS (Malvern Panalytical) (Fig. 7).

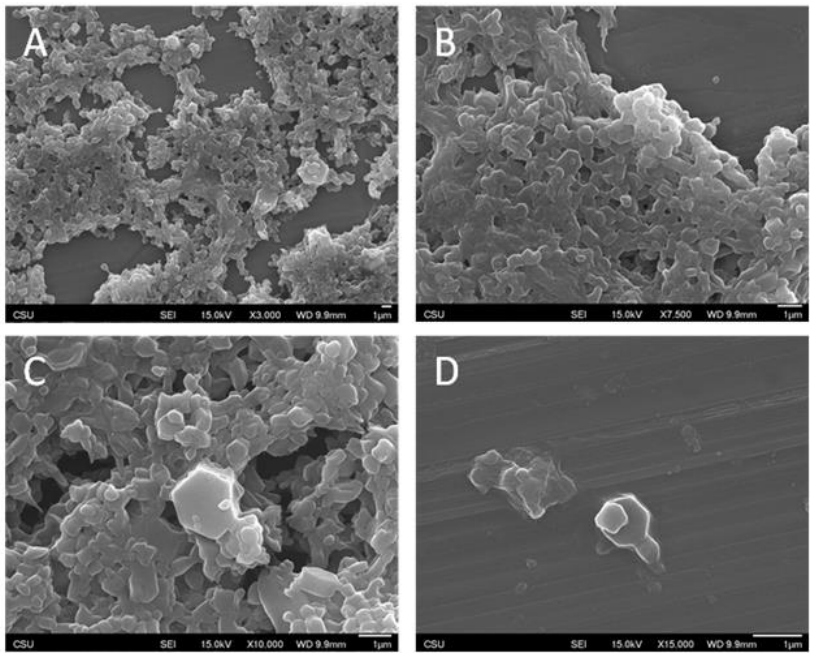

Figure (7): SEM images of nanocrystals

Measurement of guest loading in CJ microcrystals

For loading experiments, CJ microcrystal concentrations were determined using tunable resistive pulse sensing (TRPS), and concentrated microcrystals were added to fluorescently labeled DNA, RNA, or plasmid DNA, and incubated for 15 minutes at room temperature. The crystals were then pelleted by centrifugation at room temperature (2,600 g for 3:00 min), and the supernatant was pipetted into a fresh microcentrifuge tube, then spun again at >20,000 g for 5:00 minutes. The concentration of remaining DNA and RNA in the supernatant was then measured on a plate reader and compared to a standard curve. Plasmid DNA was instead quantified by measuring absorbance at 260/280 nm. All measurements were performed in triplicate.

DNA Synthesis and in vitro transcription

To obtain linearized template DNA, plasmid DNA was mini-prepped (OMEGA E.Z.N.A. Plasmid DNA Mini Kit 1 #D6943-02) and the plasmids were concentrated and eluted in nucleus Free water. The DNA concentration was quantified via NanoDrop One (Thermo Fisher Scientific). The plasmids were subsequently stored at -20°C.

Following the miniprep, we used a pair of designed forward and reverse primers to amplify a 2,000 bases long DNA template in a set of 50 µL reactions using a thermocycler MasterCycler Pro made by Eppendorf to perform Polymerase Chain Reaction (PCR). The PCR consisted of 2 steps containing 3 phases each. Prior to the temperature cycling required for annealing and extension, the mixture was heated to 98°C for 30 seconds to allow for denaturation. Following this initial denaturation, 20 cycles were administered consisting of the following steps: 10 seconds at 98°C, a 20 second 65°C annealing period- this temperature was decreased by 1°C for each repetition- and a 2 minute extension at 72°C. Following the final extension, a second round of temperature cycling was performed with a 10 second denaturation at 98°C, followed by 45°C for 20 seconds, then 72°C for 2 minutes. This was also cycled 20 times. A crude estimate for the primers' melting temperature can be calculated using the following formula (ThermoFisher: PCR cycling parameters-six key considerations for success):

$$T_m = 4(G + C) + 2(A + T)$$

As an alternative method of calculating melting temperature, since the sodium concentration could affect the primer annealing, the following formula provides a more

sophisticated approximation (ThermoFisher: PCR cycling parameters-six key considerations for success):

$$T_m = 81.5 + 16.6(log\ log\ [Na^+]\ ) + 0.41(\%GC) - \frac{675}{primer}length$$

However, a better melting temperature estimate can be computed using the Santa Lucia nearest neighbor model as made available on the (Tm Calculator | Thermo Fisher Scientific - US) website.

The produced DNA template was then digested using DPN I enzyme from NEB and incubated at 25°C for at least an hour (Fig. 8). This restriction enzyme cleaves regions of methylated nucleic acid. (New England Biolabs, #R0176L1).

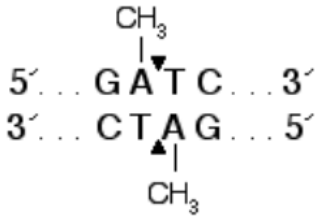

Figure (8): Location where DpnI cleaves where methylated sites are its recognition site (New England Biolabs, #R0176L)

After the digest is done, the DNA was concentrated and washed using washing buffers (PB and PE) from ZYMO Research DNA clean and concentrator kit, then quantified on the NanoDrop One. The length of the sequence was verified using a denaturing 1% TAE electrophoresis gel.

To produce the targeted 1.8 kb RNA from the amplified DNA, a reverse transcription reaction was performed wherein a T7 polymerase was used from a Promega T7 RiboMAX Express Large Scale RNA Production System kit and incubated at 37°C for around 4 hours. A DNase digest was performed to get rid of any remaining DNA. Using the Monarch kit, the RNA was concentrated, purified, and extracted which was then quantified using the NanoDrop One. The length was then verified using a denaturing 1% TAE electrophoresis gel.

RT-qPCR Hydrolysis Quantification

We developed a quantitative RT-qPCR assay per a study performed by Padhi et al. to quantify the amount of full-length intact RNA present (after elution from host crystals) using two pairs of primers that synthesize amplicons derived from both ends of the RNA sequence (5' and 3'). First, the RNA was converted to DNA via reverse transcription, which proceeds exclusively from the 3' end. The 5' end of the DNA product was read by the following primers: forward primer (5'- GAGATATACATATGGCCGAG GTGC -3') and reverse primer (5'- GCCTCTTGTCTGGAGTCTGG -3'). The 3' end was read by the following primers: forward primer (5'- GGCATGGACGAGCTGTACAA -3) and reverse primer (5'- CCCCTCAAGACCCGTTTAGA -3'). Specifically, we measured the relative expression of two amplicons derived from the 3' and 5' ends of the RNA strand.

We incubated 1.8 kbp RNA (~10^{-3} M) with CJ nanocrystals (~300 nm) overnight at 4°C for the RNA to load. The loaded nanocrystals were then transferred to two centrifugation tubes (100 kDa MWCO) from Pall Corporation. The crystals were washed three times to remove any

excess RNA by centrifugation at 20,000 rcf for 1 minute where the flow-through was collected in a 2 mL tube. This flow-through was then discarded. After the washes, 50 µL TE buffer (1 M, pH 6) was added, with one tube containing 0.1 mg/mL RNase A from OMEGA and the other being a control with no RNase A present. Both tubes were then incubated at 37°C for 15 minutes. The crystals were then washed again three times to get rid of any traces of RNases with NF water and then incubated with 20 mM ATP for roughly 60 minutes to release adsorbed RNA. The tubes were then centrifuged and the flow-through was added to a reverse transcription (RT) reaction using Invitrogen SuperScript IV kit. To set up the RT reaction, 1 µL 3' R primer (10 µM) was added to 10 µL eluted RNA and incubated at 65°C for 5 minutes. During the primer heat deactivation, RT reaction master mix was prepared by mixing 4 µL 5X buffer, 1 µL RT enzyme, 1 µL RNase Inhibitor, 2 µL 10 mM dNTP, and 1 µL NF per 20 µL reaction where the rest of the 20 µL reaction was RNA template (11 µL). The reaction was incubated at 42°C for 90 minutes then heat inactivated for 5 minutes at 70°C.

After the RT reaction is done, an RT-qPCR master mix was made using SYBR Green (Agilent, #600886) where 10 µL of SYBR green was added with (200 nM) of either 3' or 5' Forward (F) and Reverse (R) primers, template, and the reaction was upped with NF water to 20 µL volume per reaction. This brought the number of reactions to 10 where RT-qPCR was also performed on solutions that may or may not have been exposed to RNase A along with contamination control. The reason for choosing SYBR green as a dye is because of its benefits of not having a specific probe design and decrease in assay setup time and cost (Fig. 9).

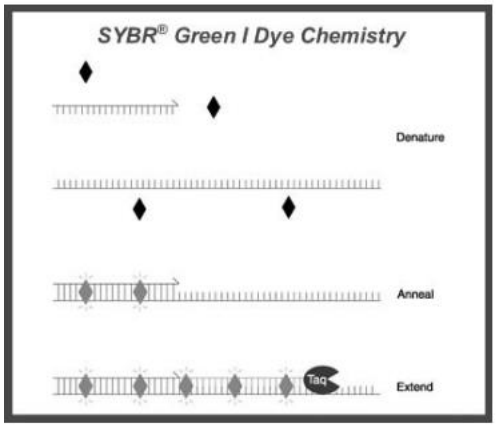

ADVANTAGES	DISADVANTAGES
Fluorescent intensity proportional to the amount of PCR products produced. Possibility of monitoring the amplification of any dsDNA. No requirement for specific probe design. Decreased assay set-up time and running costs.	No target specificity of the dye. Possibility of generation of false positive signals. Recognition of products require melting-curve analysis.

Figure (9): Benefits of using SYBER Green (33)

A qPCR experiment was also done to test the extent of hydrolysis of dsDNA (135 bp) loaded nanocrystals (Fig. 10). Similar steps to the RT-qPCR for the RNA were made where 20 µL DNA (~10^{-3} M) was incubated with nanocrystals overnight in a 4°C room. The crystals were transferred to filtered centrifugation tubes (100 kDa MWCO). The crystals were washed three times with 1 M Bis-Tris buffer (pH 6). One of the tubes contained 90 units DNase from Qiagen and was incubated at 37°C for 20 minutes. The crystals were then washed with NF water three times to remove DNase by centrifugation at max for 1 minute. After the washes, 20 mM ATP was added and allowed to incubate at room temperature. SYBER Green master mix was made with forward primer (5'- CATCACCACCATCACCAA - 3') and reverse (5' - CGTTAG GACCGTAGCGTA - 3') primers using the same format as mentioned in the RT-qPCR using a Bio-Rad CFX Opus 96 Real Time PCR.

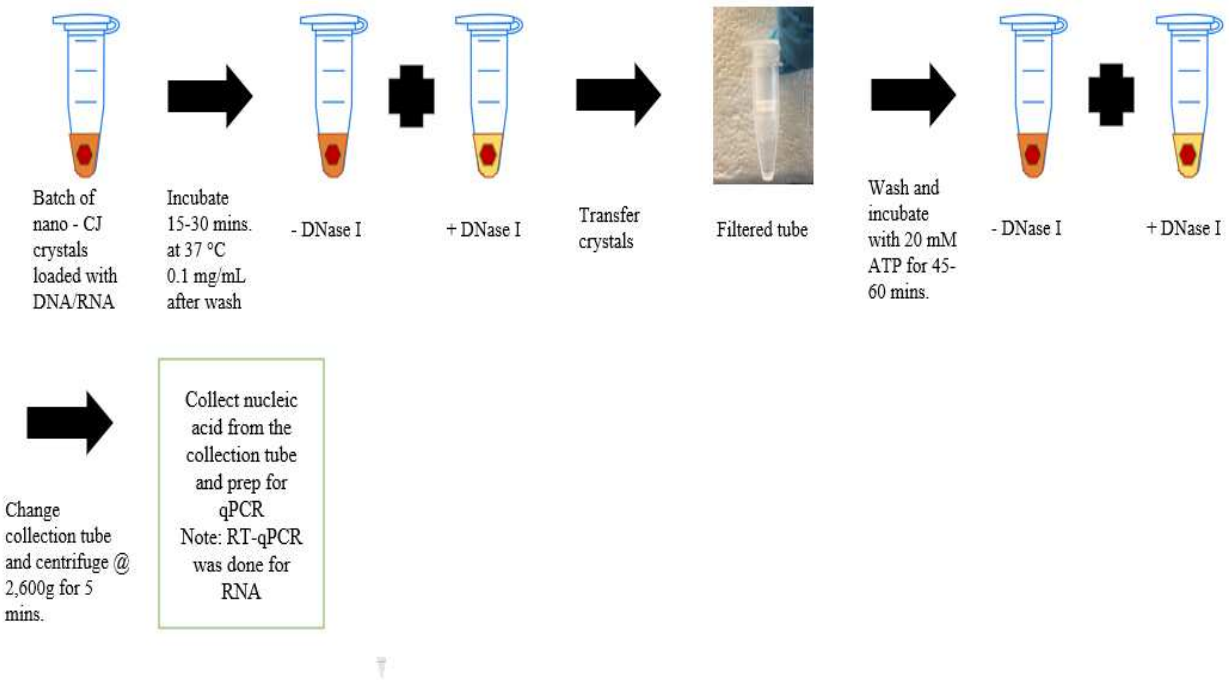

Figure (10): Illustration of the qPCR experiment workflow.

For data analysis, Agilent Aria 1.71 and Bio-Rad CFX Maestro software was used to monitor the fluorescence signal (ΔR) over the number of cycles in real time which produces an amplification plot. Using the amplification plot (Fig. 11), the initial copy number based on threshold cycle (Ct) can be quantified. The threshold is inversely proportional to the log of the initial copy number, so the higher the concentration of the template used, the earlier an observable cycle (23). In addition, these instruments provided the quantification cycle (Cq) which is the needed fractional number of cycles for which the fluorescence reaches a quantification threshold. Using the $\Delta\Delta C_t$ method and by normalizing each treatment to the 3' copy number (30). The mRNA hydrolysis can be assessed and compared through multiple treatments regardless of the RNA concentration.

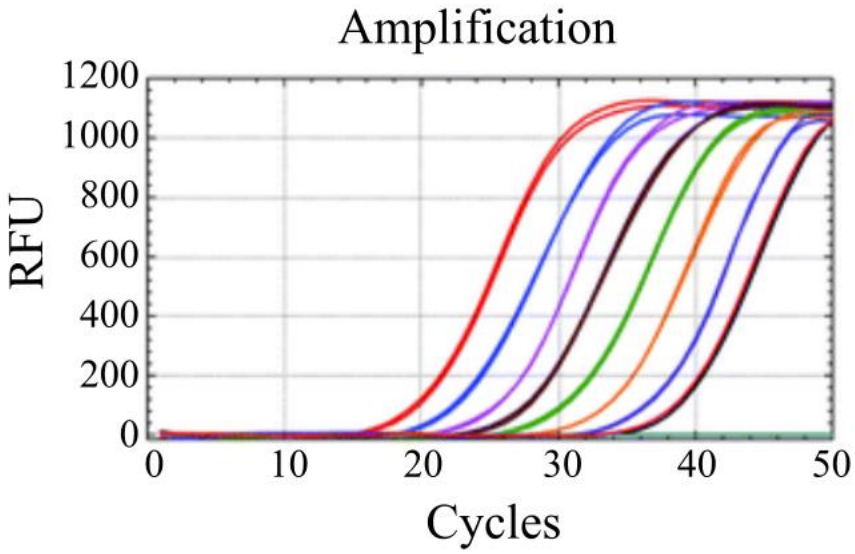

Figure (11): Example qPCR data with variable number of cycles before strong amplification (23)

The delta – delta Ct method also known as $2^{-\Delta\Delta Ct}$ method, uses the Ct values given by the thermocycler of each replicate and averages them for each sample. Calculate ΔCt for each sample ΔCt = Ct(treated sample) – Ct(control) where the control was not exposed to DNase/RNase while the treated sample was exposed to DNase/RNase. The control was chosen to be our reference sample to calculate $\Delta\Delta Ct$ for each sample $\Delta\Delta Ct = \Delta Ct(treated\ sample) - \Delta Ct(control)$. Then finally, from the $\Delta\Delta Ct$, the fold change was calculated $2^{-\Delta\Delta Ct}$.

FRET-Based ssDNA probe

A FRET – based assay was designed and implemented to test the extent of hydrolysis in guest nucleic acid inside of crystals because of the difficulty of reliably reproducing the RT – qPCR hydrolysis data. This assay was designed and performed by a PhD candidate in the Snow Lab, Alec Jones. A 30 – nt ssDNA probe which contains a 5' FAM fluorophore and a 3'

TAMRA fluorophore was ordered. In the intact probe, proximity of the TAMRA results in quenching of FAM emission (~520 nm) when illuminated with 488 nm light, resulting in low green fluorescence. In contrast, red fluorescence resulting from FRET would be observable, as the maxima emission is around ~588 nm. When hydrolysis occurs and the two fluorophores separate, a dramatic increase in the green fluorescence when excited with 488 nm light was observed, due to loss of the quenching effect. CJ crystals were incubated with the probe for 18 hours to load into the pores. The crystals were then transferred to a solution containing (0.1 mg/mL) DNase I buffer and imaged via confocal microscopy. The CJ crystals used were crosslinked with glyoxal followed by either 0.1 M hydroxylamine or ~2 mg/mL SpyCatcher – sfGFP fusion protein to block the pores to minimize or prevent hydrolysis.

Engineering of a Molecular Cap

To ensure that nucleases would be unable to diffuse into the crystal pores, we pursued a design approach which relies on physically capping the crystal pores following guest loading. Due to the arrangement of histidine tags in a six-fold radially symmetric manner, we sought a protein which formed a stable hexamer, and which could be engineered such that the histidine tags on the assembled hexamer would align with the tags of the CJ crystal, to allow the cap to be tethered in a manner similar to past guest proteins (16). Furthermore, the diameter of the assembled hexamer should be ~ 110 Å ± 10 Å, to ensure that the majority of the pore remains occluded, while remaining slightly undersized to allow it to fit (Fig. 12). As a final constraint, the protein should be easily expressed in *E. coli* and purified using metal affinity chromatography.

Based on these constraints, we identified the D2 domain from human N-ethylmaleimidesensitive factor (NSF) as favorable candidate (PDB code 1NSF). As shown in Fig. 12A and 12B, the dimensions of the assembled hexamer are ideal for obstructing the major pore of CJ crystals. Because the histidine tag was initially too short to fully interact with the histidine tag of the pore wall in a hypothetical 3D model (Fid. 12), we introduced a TEV protease recognition site between the protein sequence and the C-terminal histidine tag; this would have the added benefit of allowing rapid uncapping of the crystal. The D2 domain of human NSF was amplified from cDNA from human blood, using the following primers: NSF forward (5'-TTTTGTTTAACTTTAAGAAGGAGA TATACAATGAAACCAGCCTTTGGCACAA-3') and NSF reverse (5'-TCAGTGGTGGTGGT GGTGGTG GCCGCCCTGAAAATACAGGTTTT CGCTGCCGCCTTCTCTTAAGAGGGCC AAGAATTT-3'). The resulting 828 bp amplicon was assembled in the pSB3 backbone via splice-by-overlap extension PCR. The resulting construct was transformed into BL21-DE (3)-Gold cells. The protein was expressed and purified as described previously (43).

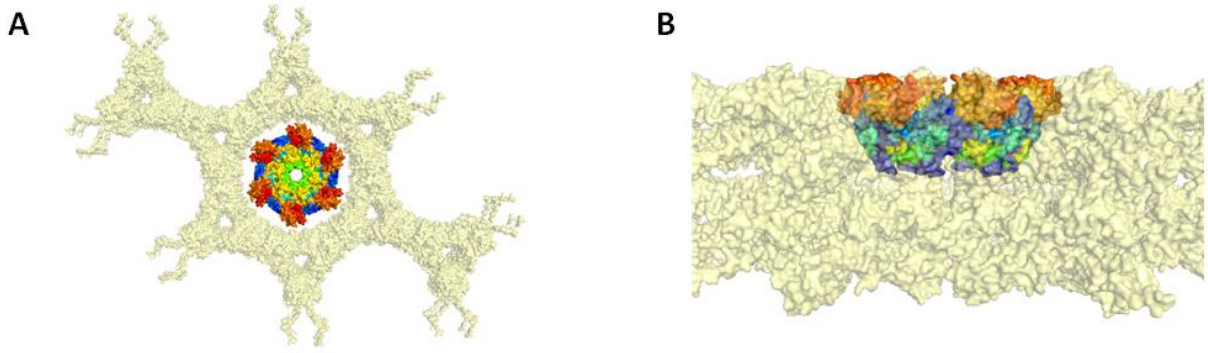

Figure (12): A. PYMOL illustration of hexameric D2 domain from N-ethylmaleimide sensitive factor (NSF) (PDB: 1NSF), relative to the CJ major pore. The diameter of the assembled hexamer is ~ 110 Å, while the CJ pore is ~130 Å. **B.** Profile view of NSF cap within the CJ pore; the assembled cap penetrates the pore to a depth of ~ 50 Å, or roughly one CJ unit cell.

Two large CJ crystals were crosslinked and soaked overnight in 1 µM hydrolysis probe (5'- TATCTCCACCATCACCAAGCTTAGTACCCGGAATA-3'). After washing and soaking in 10 mM NiSO4, one crystal was soaked in 0.5 mg/mL purified NSF for > 1 hour at room temperature. Both crystals were then washed and transferred to a new solution containing 0.1 mg/mL DNase I, and imaged directly via spinning-disk confocal microscopy. Immediately after the first frames were acquired, DNase I buffer was added to the drop containing both crystals, which were then imaged over roughly one hour.

Measure rate of release of guest nucleic acid from CJ protein crystals

The rate of release of fluorescent labeled nucleic acid from CJ crystals was quantified by measuring the fluorescence emission intensity of the crystal over time by continuously flowing different concentrations of ATP over a period of time using microfluidic devices. The nucleic acid used for this experiment was FAM – labeled ssDNA (5'- TAG GCG ACT CGA CGG TCT TAC GCG TTA CGT - 3') purchased from Integrated DNA technologies (IDT). The microfluidic devices were made of economically affordable material such as transparent polystyrene (3M transparency film for copiers PP2500) and double-sided adhesive (3M 467 MP double sided adhesive). The adhesive and polystyrene were laser cut to obtain a reservoir capacity of 8 µL, and a flow channel height (adhesive thickness) of 50 µm. Width of the flow cell (w) and the diameter of the inlet and outlet ranged between 2 - 1.4 mm, the dimensions of the reservoir were 12.5 x 12.5 mm, and the length (L) of the flow cell was 37.5 mm (Fig. 13A). The flow cell contained a blockade with a gap ranging between 0.1 – 0.04 mm to assist with keeping the crystal stationary. The reservoir has an outlet port where a paper pump (Fig. 13B) was used to sustain fluid flow.

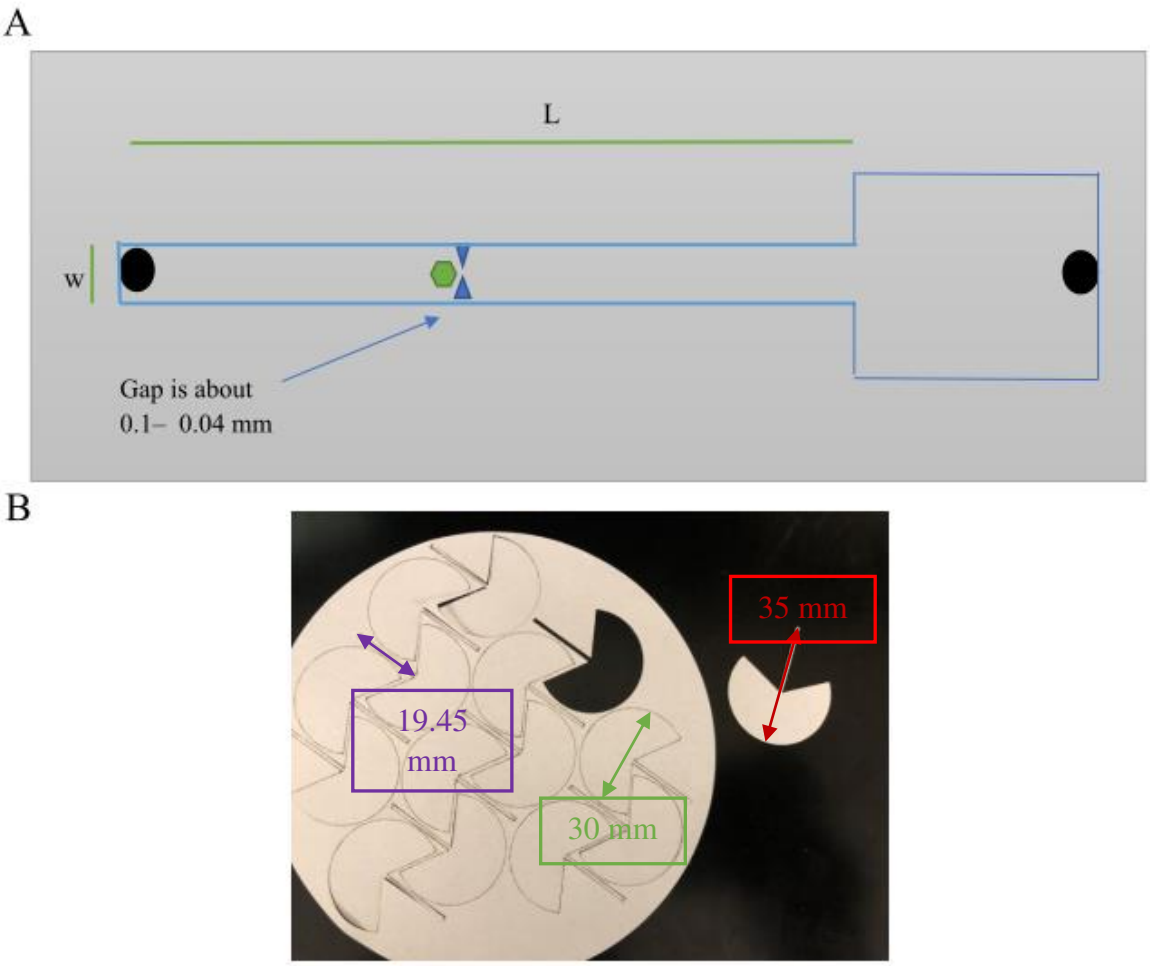

Figure (13): Illustration of the device and paper pump

ATP exists naturally in the body. The intracellular concentration of ATP in humans ranges between 1 – 10 mM (44). Therefore, we chose to test the release of the guest nucleic acid from CJ crystals by washing with 4 different concentrations of ATP (100 – µM, 2-, 8-, and 40 – mM ATP).

IV. RESULTS AND DISCUSSION

Growing CJ protein microcrystals

CJ protein was concentrated to around 35 – 50 mg/mL and stored at -20°C after expression and purification as mentioned previously. Using vapor diffusion sitting drop trials, we were able to grow crystals as large as 400 µm. We used the Gryphon liquid handling robot to screen for the optimum conditions to grow CJ protein crystals to the desired size. It was noticed that crystals grown in the salt concentration range of 3.2 – 3.6 M provided CJ protein crystals. The closer the concentration to 3.2 M the larger the crystals.

The crystals like to be in the environment they grew in. As expected, the crystals were quite unstable and would dissolve when moved to a less salty or different pH conditions within seconds (Fig. 14).

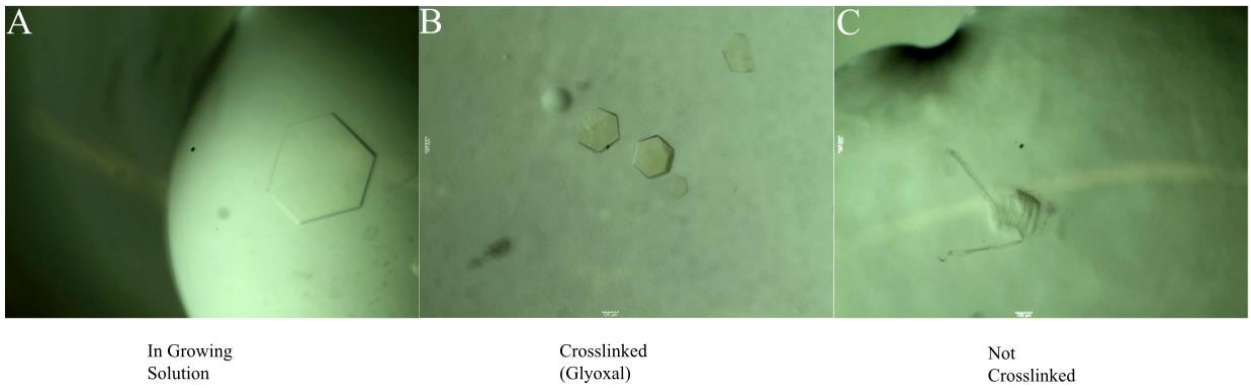

Figure (14): A. CJ crystal in its growing condition. **B.** Crosslinked crystals in water. **C.** Not crosslinked crystals in water. Scale bar = 100 µm

Batch crystallization was performed, and crystal growth conditions were optimized based on pH, precipitant concentration, temperature, PEG, and protein concentration. Of these, protein concentration was found to be a much more significant factor than any of the previous parameters. After characterizing size distribution and concentration of glyoxal-

crosslinked microcrystals using tunable resistive pulse sensing, we further validated these results by direct imaging using SEM (Fig. 15A-D). Crystal sizes obtained from SEM images (Fig. 15E) were consistent with the TRPS data (Fig. 15F) in terms of the microcrystal size distribution (mean size = 367 nm), although the nanocrystal agglomeration was a hindrance towards definitive size characterization. It was difficult to observe the distinctive hexagonal crystal habit until crystal diameters exceeded 500 nm; below this size, CJ nanocrystals appeared to be amorphous.

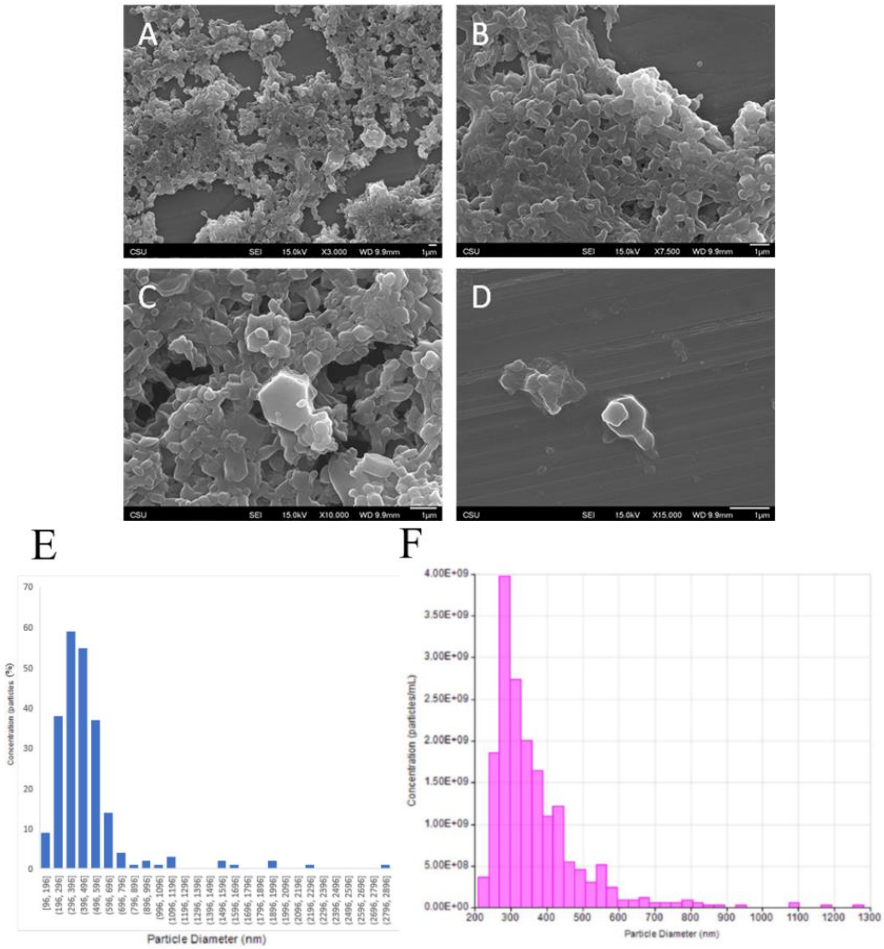

Figure (15): A-D. SEM images of CJ micro- and microcrystals. Scale bar = 1 µm. **E**. Size data of crystals as measured from SEM images using ImageJ. **F**. Size data of crystals obtained using tunable resistive pulse sensing (TRPS)

CJ crystals adsorb, retain, and release guest DNA, RNA, and proteins

CJ crystals adsorb, retain, and release guest DNA, RNA, and proteins

CJ crystals possess large pores (~13 nm diameter), which allows them to intake a wide range of guest molecules such as DNA, RNA, and proteins. We tested first their ability to load and release guest molecules; three CJ crystals were loaded with (1 μM) FAM – labeled ssDNA 30 nt long (5'- TAG GCG ACT CGA CGG TCT TAC GCG TTA CGT -3') over 15 minutes and we were able to visualize the loading in real time. The crystals were then left to incubate at about 4°C overnight to get complete loading (Fig. 16A). The next day, the three CJ crystals were washed with 8 mM ATP where the guest nucleic acid was visualized in a steady release over 15 minutes. The crystals were then left to incubate at about 4°C overnight in 40 mM ATP to get a complete release (Fig. 16B). However, in panel 17B at t = 20 hours, we can see the borders of the crystal remain fluorescent which could indicate tightly bound FAM – labeled ssDNA remaining inside the crystal or on the crystal surface.

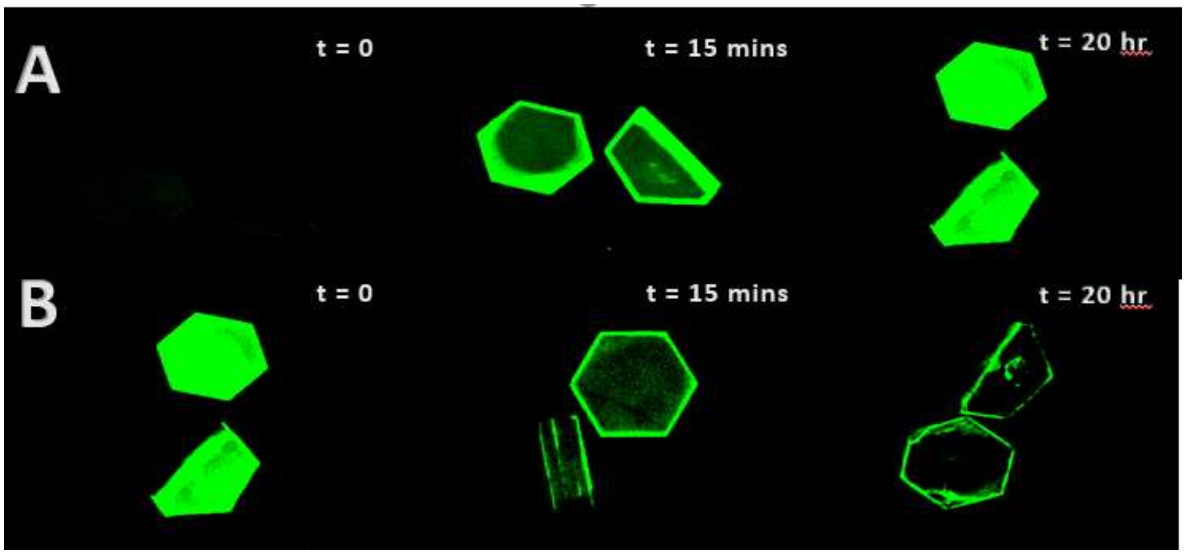

Figure (16): A. Loading the crystal with FAM – labeled DNA over time. **B.** Release of FAM – labeled DNA over time using 40 mM ATP.

We then sought to test the RNA and DNA adsorptive capacity of CJ microcrystals by incubating increasing concentrations of crystals with fixed concentrations of FAM-labeled, 19-bp anti-mCherry siRNA (300 nM) (5'- CUC CUU GAU GAU GGC CAU G -3'), or 5.8 kbp plasmid DNA (~17.9 ng/uL). As shown in figures 18C and 3E, a linear increase in microcrystal concentration correlated with a linear decrease in supernatant concentration for both species, following a 30 minute incubation at room temperature. From this data, we were able to quantify the average number of siRNA or plasmid molecules adsorbed per microcrystal (14,900 ± 720 copies of siRNA, or 353 ± 80 copies of plasmid, per crystal). In addition to passive adsorption of nucleic acids, we were also able to demonstrate adsorption and functional activity of adsorbed enzyme. By measuring chemiluminescence via plate reader, we observed that the CJ nanocrystals were able to retain guest Nanoluciferase, following multiple washes in acetate or Tris buffers at varying pH values (Fig. 17A). Furthermore, we were able to directly monitor chemluminescence in a large CJ crystal, via confocal imaging, over a ~12.5 minute window, following addition of 50 μM furimazine.

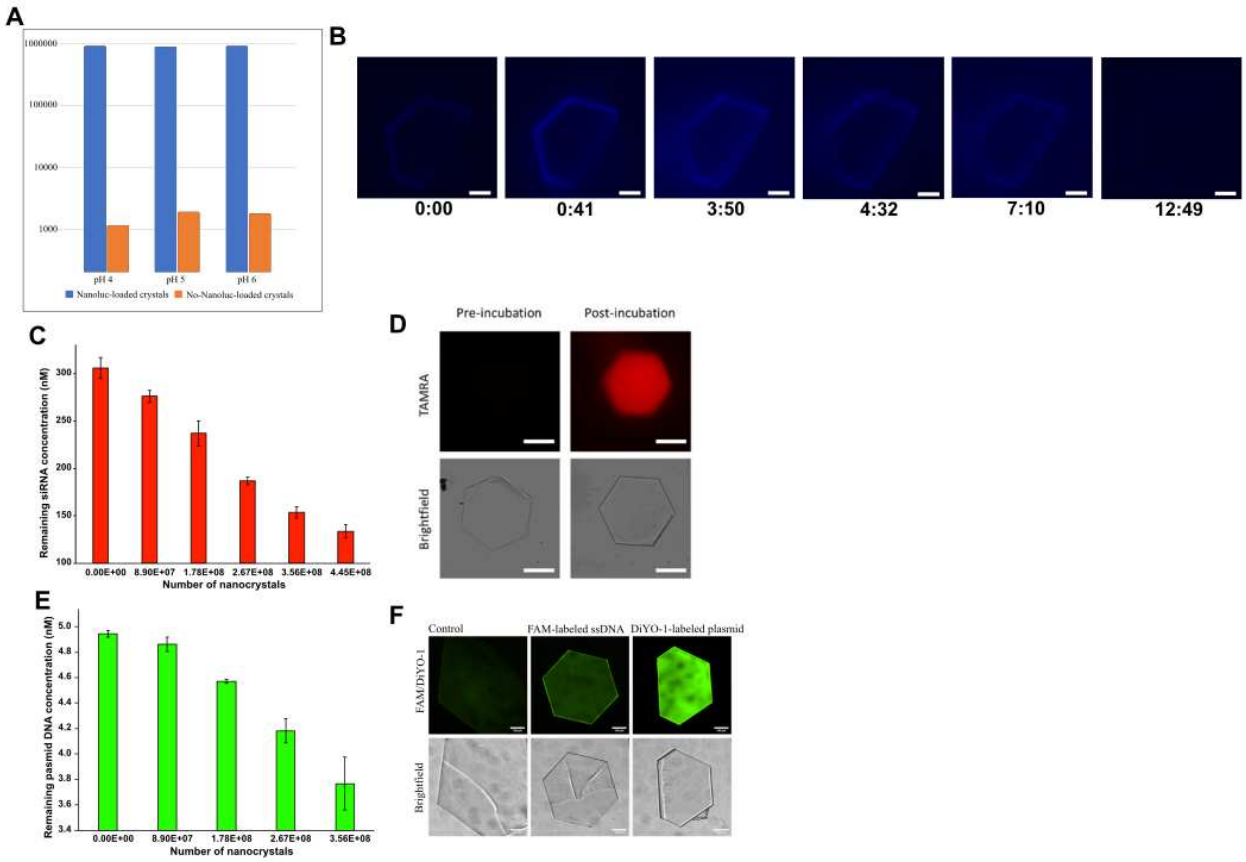

Figure (17): A. Relative luminescence for Nanoluc-loaded CJ microcrystals, stored at pH 4, 5, or 6 (blue bars), compared with unloaded crystals (orange bars); **B**. Time course confocal images showing Nanoluciferase activity in a large crystal (top), over ~13 minutes, compared with an unloaded control crystal (bottom) (scale bar = 100 µm); **C**. Supernatant concentrations of FAM-labeled siRNA, after incubating 300 nM siRNA with increasing concentrations of crystals; **D**. Confocal images of a large CJ crystal, demonstrating loading of a TAMRA-labeled, 21 nt siRNA; **E**. Supernatant concentrations of plasmid DNA, after incubating ~5 nM plasmid DNA with increasing concentrations of crystals; **F**. Confocal images of a large crystal, demonstrating successful loading of DiYO-labeled plasmid DNA and FAM-labeled ssDNA.

DNA synthesis and in vitro transcription

First, we Mini-Prepped PNZ108 plasmids in which we amplified a region (2,000 bp) using PCR. Next, we used the linear DNA as a template to transcribe intact RNA (1,800 bp) and used 1x TAE gel electrophoresis to ensure that we obtained the targeted length. Five PCR reactions were performed to amplify the DNA template of the PNZ108. The five reactions were

verified on agarose gel (Fig. 18). The samples were then cleaned and concentrated and stored in the -20 °C or 4 °C for short term storage.

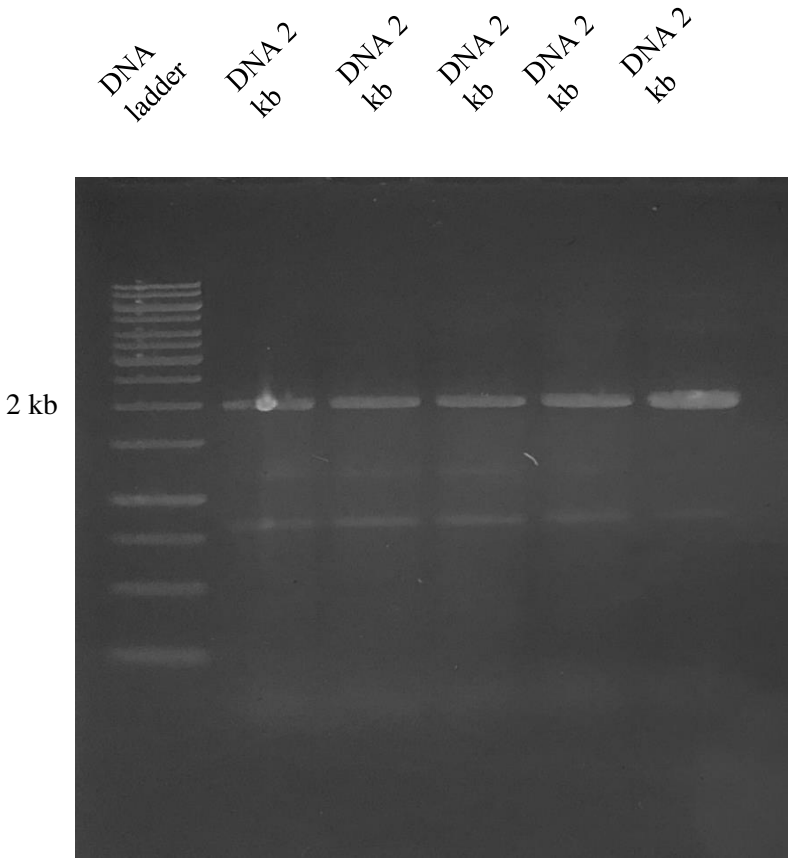

Figure (18): PCR amplification of PNZ108 template

With purified 2,000 kb DNA in hand, *in vitro* transcription was performed to obtain 1.8 kb RNA. The RNA product was verified on a denaturing RNA electrophoresis 1x TAE gel using formaldehyde (Fig. 19). Formaldehyde acts as a denaturing agent for RNA during agarose gel electrophoresis, which also helps maintain RNA integrity during gel handling and separation (26). The rest of the RNA sample was aliquoted into 5 µL aliquots and stored at -80°C.

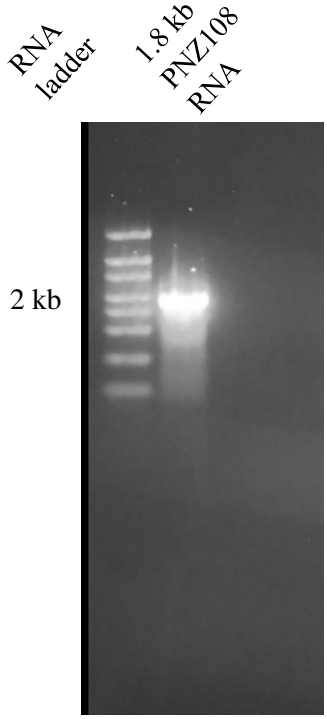

Figure (19): *In vitro* transcription product PNZ108 2 kb RNA

Quantifying RNA hydrolysis in loaded nanocrystals

We designed two pairs of primers for amplifying the 5' and 3' regions. A standard curve was performed to test the quality of the primers (Fig. 20A). These primer pairs had close reaction efficiencies (95.4% and 96.0% for 5' and 3' amplicons) (Fig. 20B).

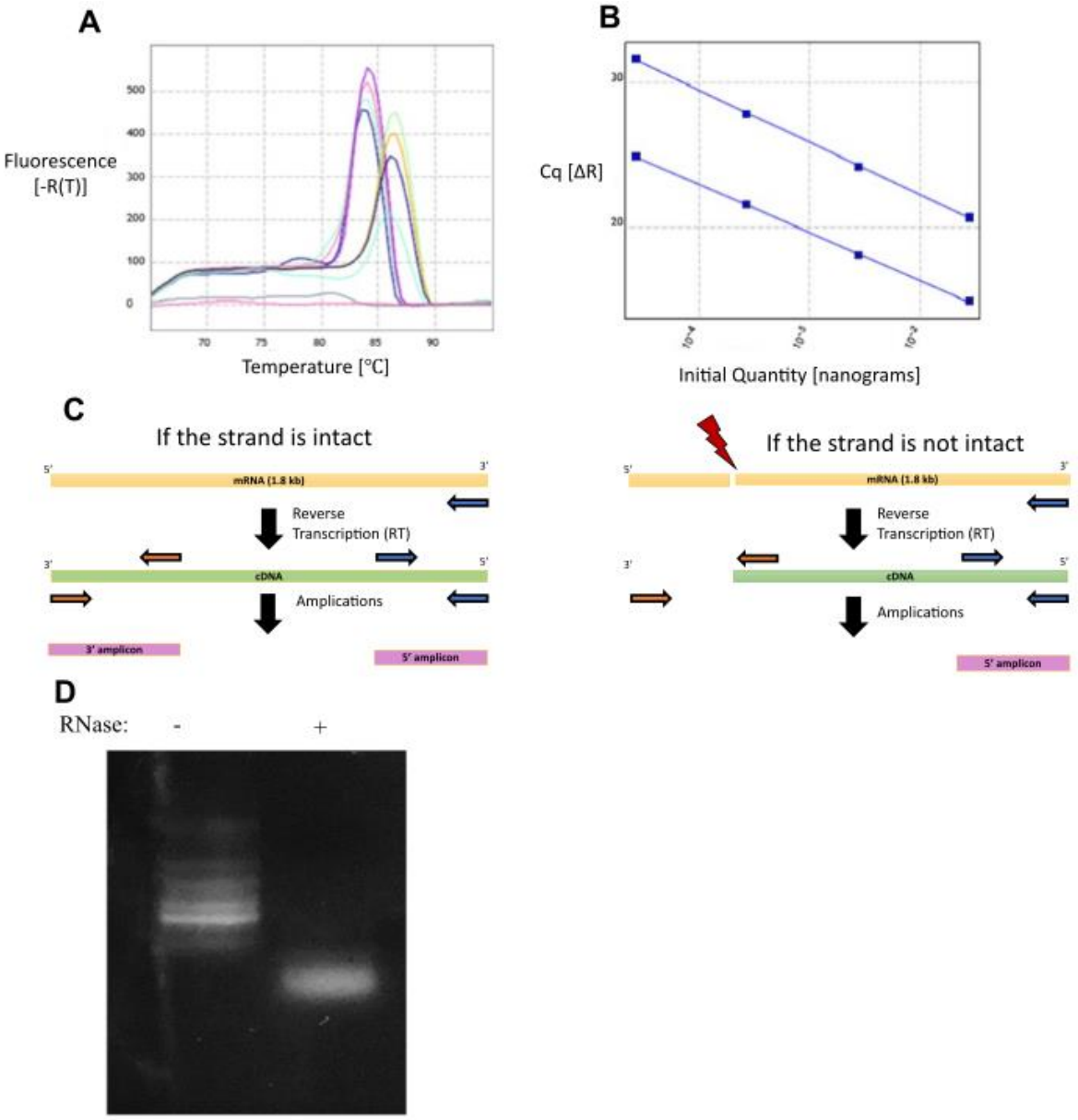

Figure (20): A. Melt curve analysis demonstrating distinct peaks for amplicons within 5' and 3' regions of the 1.8 kbp mRNA. **B**. Standard curve for 3' (upper) and 5' (lower) amplicons; R^2 = 0.998 for both. **C**. Method for relative quantification of hydrolysis, by measuring the ratio of 3' to 5' amplicons in reverse-transcribed mRNA from treated and untreated crystals. **D**. Denaturing gel demonstrating size shift in mRNA samples (375 ng per well), treated with or without RNase A (0.1 mg/mL).

Pairs of primers were designed to amplify small regions (~150 bp) at opposite ends of the RNA sequence (~1.8 kbp). Following exposure of nanocrystals loaded with mRNA to nucleases, and RNA release via incubation in 20 mM ATP; the sample RNA was reverse transcribed using

the 3’ primer to produce cDNA (of varying size due to the potential hydrolysis). We used qPCR to compare the number of intact 3’ amplicons and the number of intact 5’ amplicons, and to calculate the relative fold change of intact RNA in the sample, using the ΔΔCt method. In other words, using the $\Delta\Delta C_t$ method, mRNA hydrolysis can be measured from the 5’ amplicon quantity relative to the 3’ amplicon quantity (Fig. 20C). After measuring the difference between the 5’ and 3’ cycle thresh holds for each sample (+/- RNase A), the difference in the resulting values was used to determine the fold change by taking the antilog ($2^{-\Delta\Delta Ct}$). We observed a decrease in intact RNA following RNase exposure (Fig. 21A), suggesting that the crosslinked nanocrystals were not sufficient to protect guest RNA on their own. As a control, the activity of RNase A and DNase I used in this experiment were independently validated by gel electrophoresis (Fig. 21B). Specifically, released mRNA was imaged on a denaturing gel (1% agarose – TAE) containing 1.5% household bleach (Fig. 20D). However, it was difficult to reliably reproduce the data that was produced from the RT – qPCR, so we instead developed a FRET – based probe method to observe hydrolysis inside the crystal.

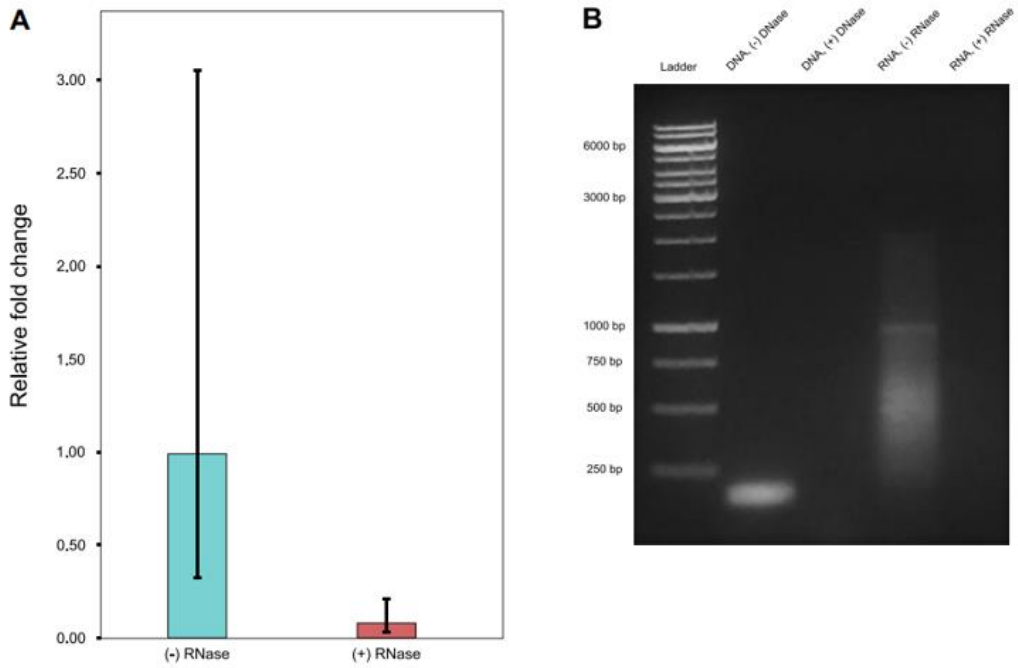

Figure (21): A. Guest RNA was significantly degraded following incubation of loaded CJ nanocrystals in 0.1 mg/mL RNase A for 30 minutes. Fold change was calculated using the ΔΔCt method. **B**. Gel electrophoresis confirming activity of DNase I and RNase A used in the experiments.

We next attempted to monitor hydrolysis directly in the crystal using a FRET-based probe (Fig. 22A) consisting of a 35 – nt ssDNA probe that contained 5' FAM and 3' TAMRA fluorophores. After loading this probe into a large CJ crystal, the crystal was transferred to a solution containing DNase I buffer and imaged via confocal microscopy. After adding DNase I to a final concentration of 0.1 mg/mL, followed by addition of DNase I buffer after ~ 20 minutes, we observed a sharp increase in FAM fluorescence within the crystal, indicating guest hydrolysis. Together with the data obtained by RT-qPCR in the RNA-loaded microcrystals, these results indicated that the crystal scaffold alone was insufficient to protect guest DNA or RNA from nucleases.

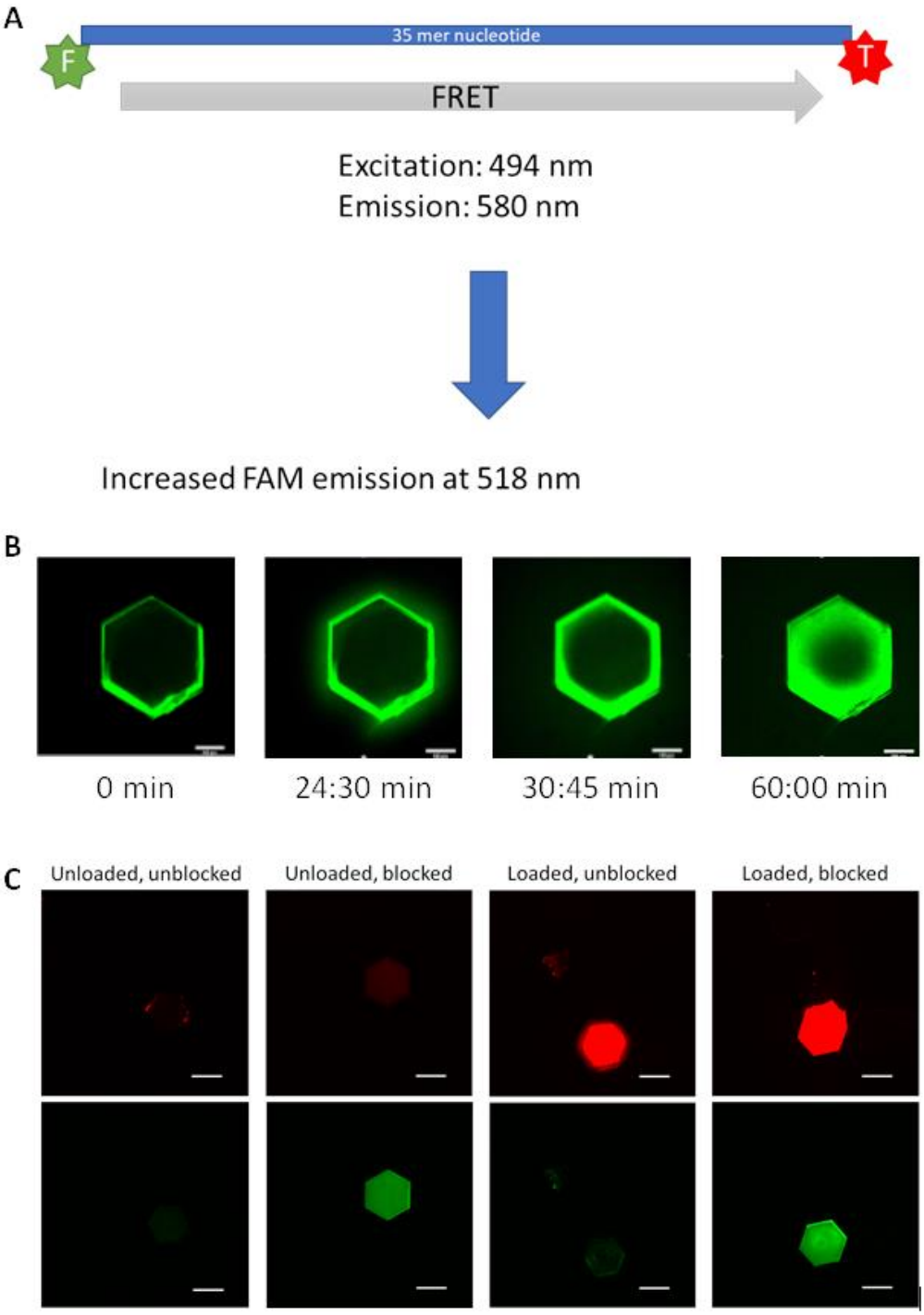

Figure (22): A. Illustration of FRET assay principle; in the absence of hydrolyzing conditions, green fluorescence of FAM is quenched by TAMRA fluorophore at the 3' end of the molecule. **B**. Time course series demonstrating hydrolysis of guest DNA, following DNase I activation at 20 minutes; **C**. Confocal images for loaded or unloaded crystals which were quenched in either 0.1 M hydroxylamine, or blocked with ~2 mg/mL SpyCatcher-sfGFP fusion protein, following crosslinking. Scale bars = 100 µm.

CJ pores can be protected by capping proteins

As observed in figure 23, green fluorescence, indicating guest hydrolysis, was observed in the uncapped crystal (left), but not in the capped crystal (right), indicating that the NSF cap conferred protection against environmental nucleases. We have successfully replicated these results in a different pair of CJ crystals, and are currently pursuing direct visualization of the capped pores using atomic force microscopy, in addition to recapitulating these results in microcrystals. We have also recently ordered the RNA equivalent of this DNA probe and intend to use it to monitor RNA hydrolysis under physiological pH conditions for both unmodified and modified CJ crystals.

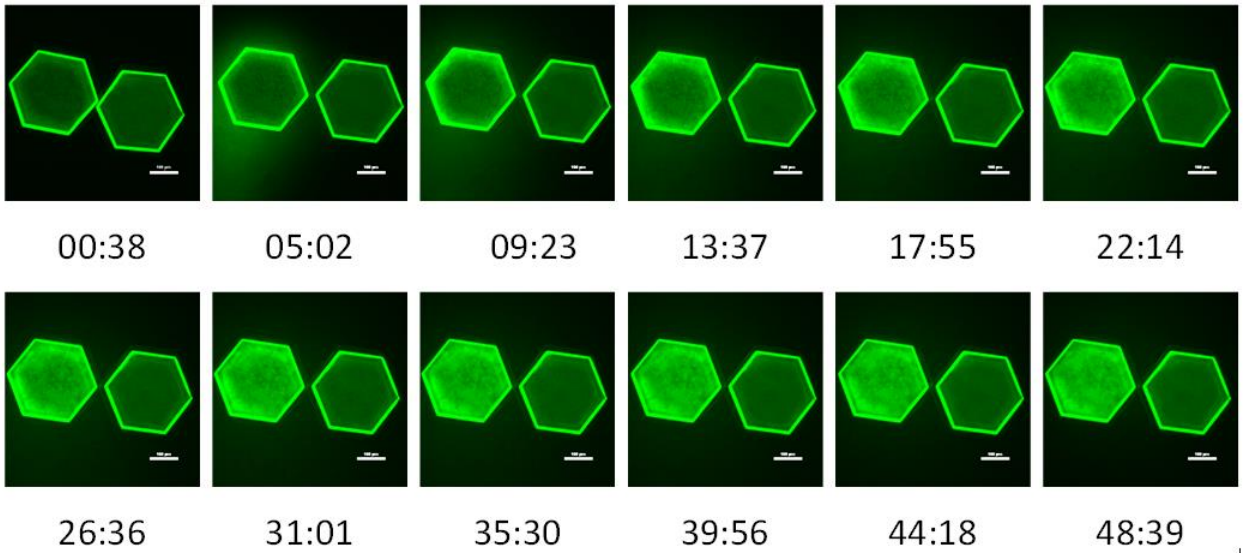

Figure (23): *In situ* FRET-based monitoring of hydrolysis of a single-stranded DNA in the presence of DNase I, for a capped (right) and uncapped (left) crystal. Acquisition time is indicated beneath each panel, in mm:ss format; scale bar = 100 µm. Green fluorescence indicates guest hydrolysis.

Measurement of rate of release of DNA based on ATP concentration from CJ crystals

A functional cargo molecule is only useful if it can be released. To demonstrate controlled release, we developed an in-house flow cell device to measure intensity over time using fluorescent DNA to show loading and release under the confocal microscope. We used the flow cell to visualize how long it takes to load the CJ protein crystals and release the load using different concentrations of adenosine triphosphate (ATP), below and above the concentration of ATP in the cellular level where it ranges between 1 - 10 mM (44). Specifically, the CJ protein crystal was washed with a range of different ATP concentrations: 0, 0.1-, 2-, 8-, and 40 – mM where 0 mM was Nucleus Free (NF) water (Fig. 24A). The crystal was prewashed with 8 mM ATP for about 5 - 6 minutes then followed by FAM labelled DNA loading for 48 minutes whereupon it was visually completely green (Fig. 24B), but the intensity was increasing indicating that the loading was still occurring. The crystal was then washed with NF water for about 10 minutes followed by washing with 0.1-, 2-, 8-, and 40 – mM ATP for 30 minutes on each concentration. The entire process of releasing the guest DNA was 2 hours long. To our surprise, the FAM labelled DNA was not completely released even after exposing the crystal to a very high concentration of ATP (40 mM) with a good fraction of the guest DNA remaining in the crystal. Additional work remains in characterizing guest loading and release for different crystal sizes and aspect ratios.

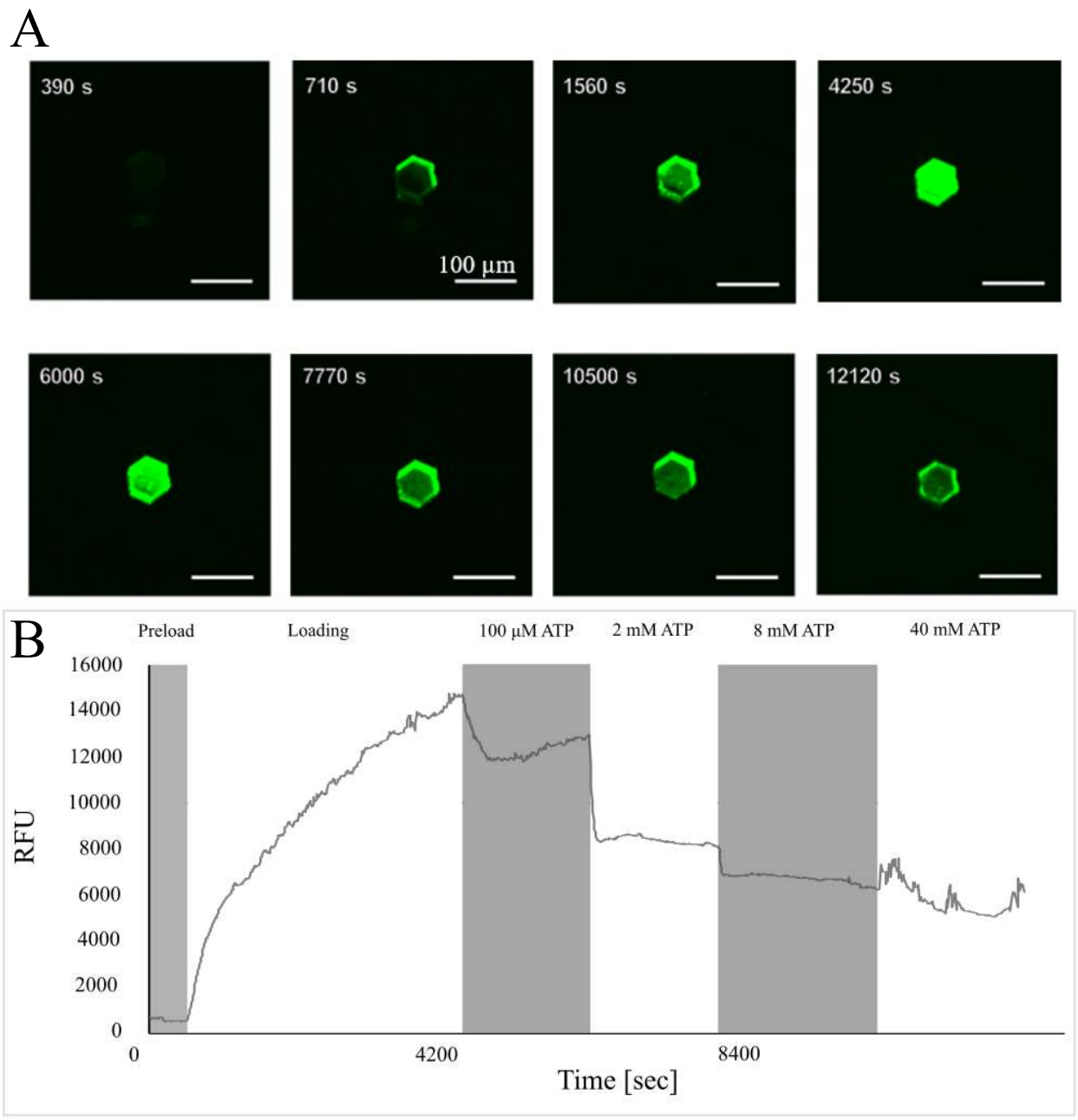

Figure (24): **A.** Direct imaging of a large CJ crystal loading during loading and release of a FAM-labeled ssDNA (30 nucleotide). Complete saturation of the crystal is observed after approximately 1 hour. Release of guest DNA was performed by washing successively higher concentrations of ATP (up to 40 mM). **B**. Relative fluorescence values over the entire crystal were obtained over the course of loading and ATP-mediated release. Intervals are demarcated by alternating white and gray-shaded regions on the graph; after loading, crystal was washed with increasing concentrations of ATP (0.1 mM to 40 mM).

Surprisingly, we consistently observed a modest increase in fluorescence following ATP washing; we hypothesize that, because the crystal was imaged in a single z-plane over time, the initial ATP may have increased the rate of transport of fluorescently bound DNA further into the crystal. Alternatively, the increase in fluorescence may be due to incomplete washing of the crystal following loading. Finally, ATP might authentically increase the affinity of the crystal for the oligonucleotide via an unknown mechanism. In any event, we consistently observed that guest DNA failed to completely release, even after washing with 40 mM ATP for several minutes.

Finally, to assess whether the crystals display hysteresis with respect to guest loading and release, we monitored three crystals over four rounds of loading and release (Fig. 25A, B). We observed that guest DNA adsorption accumulated over time, owing to incomplete release of guest DNA between each cycle (repeated exposure to 40 mM ATP). We hypothesize that a fraction of the adsorbed guest is bound much more strongly, while weakly bound DNA was released in the presence of ATP, whereupon it can re-adsorb at a more favorable site following release.

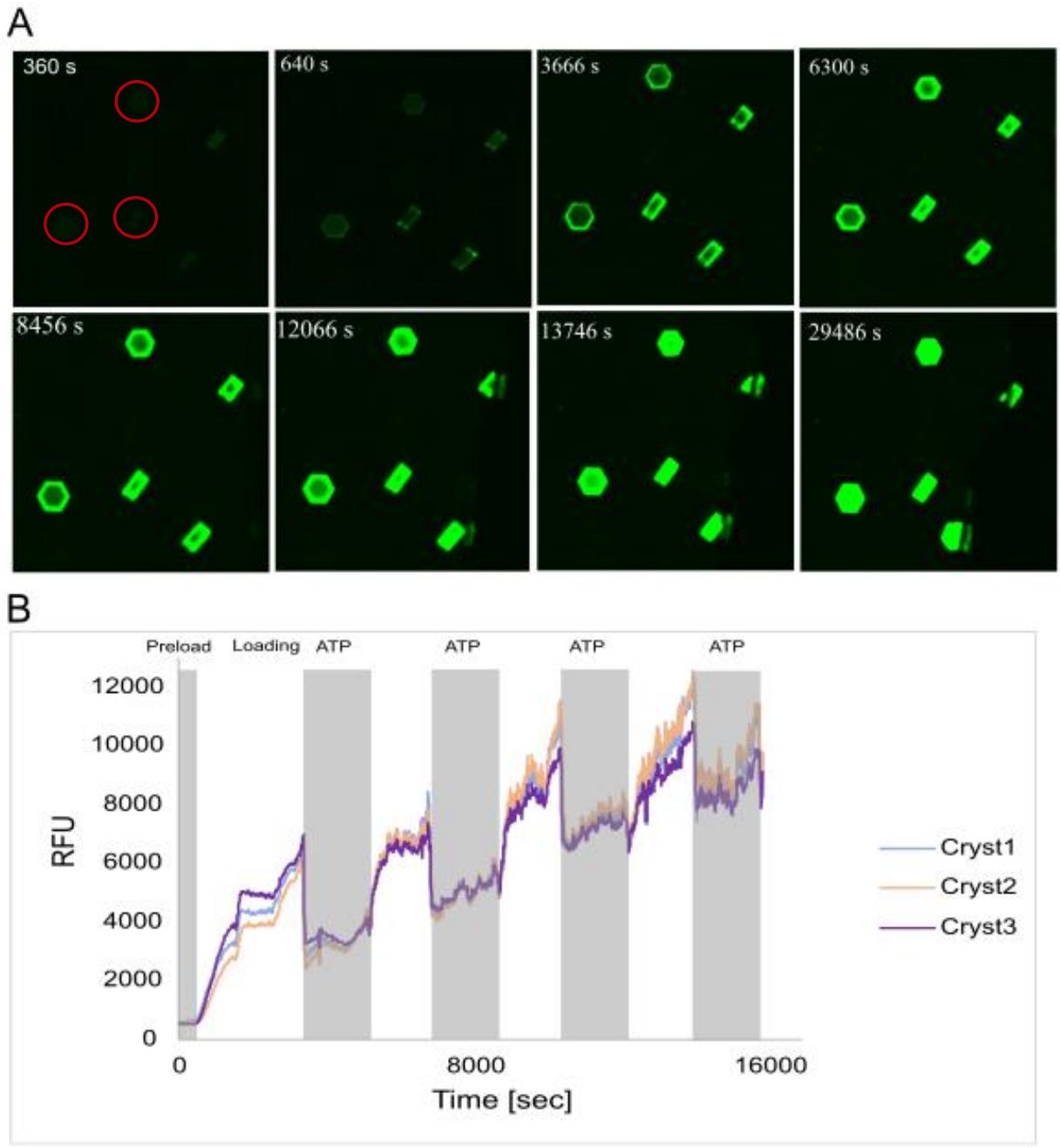

Figure (25): Quantitative data demonstrating four cycles of loading and release for three crystals (circled in the upper left panel A).

V. CONCLUSION

Porous nanomaterials have been in high demand in therapeutic and medical applications as a method of delivering therapeutic agents into the body safely and enabling targeted delivery of the loaded therapeutic. Engineered porous protein crystal have been evaluated as a nucleic acid delivery matrix. Specifically, CJ crystals were grown and their stability outside of the growth conditions significantly improved through chemical crosslinking methods such as glyoxal and EDC. In addition, we have shown CJ protein crystals' ability to adsorb guest macromolecules, which opened the possibility of using these crystals for drug delivery. We were able to grow CJ protein crystals in the nanoscale (~300 nm) enabling future uses in the human body. After showing that the CJ protein crystals size was tunable, and that it was feasible to grow them with nanoscale sizes, we evaluated the CJ nanocrystals' ability to adsorb and retain nucleic acids and proteins. The amount of guest material adsorbed was dependent on the quantity of crystals present, demonstrating a consistent adsorption per unit crystal mass. We then evaluated the CJ protein crystals' ability to protect the loaded NA guest under harsh environmental conditions and with the presence of nucleases which showed that the crystals require additional optimization to minimize/prevent hydrolysis within the pores. The high level of observed hydrolysis demonstrated the need for a method to prevent nucleases from accessing the nanopore interior. Therefore, we implemented a strategy that would cap the pores with a well-fitting protein and prevent the entrance of nucleases. This increases the ability of the crystal to protect the loaded guest within the pores. Lastly, to be of use as a drug delivery medium, the nanomaterial must be able to release the drug. Therefore, we measured the CJ protein nanocrystals' release rate in the presence of different concentrations of ATP. ATP was chosen for its ability to competitively bind within the crystalline pores, displacing the guest nucleic acid.

Additionally, ATP is a possible release factor because it is found in the human body. To visualize DNA release in real time, an affordable and easily constructed multi – layered flow cell microfluidic device was designed and assembled using transparency film and double-sided adhesive, wherein a fluorescently labeled DNA was flowed through the cell followed by ATP washes of various concentrations. Loading and release were imaged using spinning disk confocal microscopy. The release rate of fluorescent labeled nucleic acid was measured based on the ATP concentration by measuring the fluorescence emission intensity of the crystal over time. However, the protein crystals strongly retained ssDNA, even in the presence of ATP. This leads to an incomplete release and residual fluorescence. More tests will be required to fully understand the biophysics of nucleic acids confined within the host crystal nanopores.

RECOMMENDED FUTURE WORK

Cationic interactions involvement in CJ loading

Further studies will be necessary to fully understand the loading of DNA into CJ protein crystals. For example, it would be helpful to understand the effects of metals such as magnesium, zinc, or nickel on the crystal nanopore environment electronic state and how the presence of these cations affects nucleic acid's ability to adsorb onto and transit the nanopores. Furthermore, testing is needed to determine if the metals have any relationship to why the crystal does not release its load completely when washed with ATP.

Animal testing

Testing and evaluating the CJ protein crystals as a drug delivery method on rats would tell us a great deal about how well the crystals work in a living organism as compared to previous *in vitro* tests. Checking for crystal accumulation in any organs of the rats, persistence in the digestive system, and whether intact cargo DNA can be recovered from feces would inform us as to the feasibility of using crystals for oral delivery of therapeutics.

In addition to testing oral delivery, testing intravenous delivery and validating the crystals' ability to distribute in the blood would yield useful information. It would be informative to assess the degree of distribution throughout the vasculature.

Designing and developing microfluidic devices to grow nanocrystals

To maximize the production of CJ nanocrystals and to maximize repeatable growth of crystals with effective size control it would be helpful to devise a continuous flow crystallization process. For example, a Y – shaped serpentine microfluidic device may allow rapid consistent solution mixing compared to regular Y – shaped devices. The process of growing protein nanocrystals in microfluidic devices could be further automated using the syringe pump and automated via integration of crosslink and quench. This approach could potentially optimize micro/nanocrystal growth compared to the batch crystallization, minimizing aggregation and crystal accumulation which would facilitate downstream biomedical use (e.g. transport in the blood).

VI. REFRENCES

1. Aranda, P. S., LaJoie, D. M., & Jorcyk, C. L. (2012). Bleach gel: A simple agarose gel for analyzing RNA quality. *ELECTROPHORESIS*, *33*(2), 366–369. https://doi.org/10.1002/elps.201100335

2. Basu, S. K., Govardhan, C. P., Jung, C. W., & Margolin, A. L. (2004). Protein crystals for the delivery of biopharmaceuticals. *Expert Opinion on Biological Therapy*, *4*(3), 301–317. https://doi.org/10.1517/14712598.4.3.301

3. Brader, M. L., Sukumar, M., Pekar, A. H., McClellan, D. S., Chance, R. E., Flora, D. B., Cox, A. L., Irwin, L., & Myers, S. R. (2002). Hybrid insulin cocrystals for controlled release delivery. *Nature Biotechnology*, *20*(8), 800–804. https://doi.org/10.1038/nbt722

4. Bernhardt, H. S., & Tate, W. P. (2012). Primordial soup or vinaigrette: did the RNA world evolve at acidic pH? *Biology Direct*, *7*(1), 4. https://doi.org/10.1186/1745-6150-7-4

5. Chin, C. D., Laksanasopin, T., Cheung, Y. K., Steinmiller, D., Linder, V., Parsa, H., Wang, J., Moore, H., Rouse, R., Umviligihozo, G., Karita, E., Mwambarangwe, L., Braunstein, S. L., van de Wijgert, J., Sahabo, R., Justman, J. E., El-Sadr, W., & Sia, S. K. (2011). Microfluidics-based diagnostics of infectious diseases in the developing world. *Nature Medicine*, *17*(8), 1015–1019. https://doi.org/10.1038/nm.2408

6. Chung, E. J., Leon, L., & Rinaldi, C. (2019). *Nanoparticles for Biomedical Applications: Fundamental Concepts, Biological Interactions and Clinical Applications (Micro and Nano Technologies)* (1st ed.). Elsevier.

7. Coffin, J. M., Hughes, S. H., & Varmus, H. E. (Eds.). (1997). *Retroviruses*. Cold Spring Harbor Laboratory Press.

8. Didenko, V. V. (2001). DNA Probes Using Fluorescence Resonance Energy Transfer (FRET): Designs and Applications. *BioTechniques*, *31*(5), 1106–1121. https://doi.org/10.2144/01315rv02

9. Dua, K., Mehta, M., Pinto, T. D. J. A., Pont, L. G., Williams, K. A., & Rathbone, M. (2021). *Advanced Drug Delivery Systems in the Management of Cancer*. Academic Press.

10. Fabre, A. L., Colotte, M., Luis, A., Tuffet, S., & Bonnet, J. (2013). An efficient method for long-term room temperature storage of RNA. *European Journal of Human Genetics*, *22*(3), 379–385. https://doi.org/10.1038/ejhg.2013.145

11. Gopinath, S. C. B., & Gang, F. (2020). *Nanoparticles in Analytical and Medical Devices* (1st ed.). Elsevier.

12. Hartje, L. F., Bui, H. T., Andales, D. A., James, S. P., Huber, T. R., & Snow, C. D. (2018). Characterizing the Cytocompatibility of Various Cross-Linking Chemistries for the Production of Biostable Large-Pore Protein Crystal Materials. *ACS Biomaterials Science & Engineering*, *4*(3), 826–831. https://doi.org/10.1021/acsbiomaterials.8b00023

13. Hartje, L. F., & Snow, C. D. (2018). Protein crystal based materials for nanoscale applications in medicine and biotechnology. *WIREs Nanomedicine and Nanobiotechnology*, *11*(4). https://doi.org/10.1002/wnan.1547

14. He, X., Zhao, Y., He, D., Wang, K., Xu, F., & Tang, J. (2012). ATP-Responsive Controlled Release System Using Aptamer-Functionalized Mesoporous Silica Nanoparticles. *Langmuir*, *28*(35), 12909–12915. https://doi.org/10.1021/la302767b

15. Hossbach, M., Gruber, J., Osborn, M., Weber, K., & Tuschl, T. (2006). Gene Silencing with siRNA Duplexes Composed of Target-mRNA-Complementary and Partially Palindromic or Partially Complementary Single-Stranded siRNAs. *RNA Biology*, *3*(2), 82–89. https://doi.org/10.4161/rna.3.2.3110

16. Huber, T. R., Hartje, L. F., McPherson, E. C., Kowalski, A. E., & Snow, C. D. (2016). Programmed Assembly of Host–Guest Protein Crystals. *Small*, *13*(7), 1602703. https://doi.org/10.1002/smll.201602703

17. Huber, T. R., McPherson, E. C., Keating, C. E., & Snow, C. D. (2017). Installing Guest Molecules at Specific Sites within Scaffold Protein Crystals. *Bioconjugate Chemistry*, *29*(1), 17–22. https://doi.org/10.1021/acs.bioconjchem.7b00668

18. Jain, K. (2009). Role of nanobiotechnology in the development of personalized medicine. *Nanomedicine*, *4*(3), 249–252. https://doi.org/10.2217/nnm.09.12

19. Jen, A., & Merkle, H. P. (2001). Diamonds in the rough: protein crystals from a formulation perspective. *Pharmaceutical research*, *18*(11), 1483–1488. https://doi.org/10.1023/a:1013057825942

20. Kowalski, A. E., Johnson, L. B., Dierl, H. K., Park, S., Huber, T. R., & Snow, C. D. (2019). Porous protein crystals as scaffolds for enzyme immobilization. *Biomaterials Science*, *7*(5), 1898–1904. https://doi.org/10.1039/c8bm01378k

21. Kulkarni, J. A., Witzigmann, D., Thomson, S. B., Chen, S., Leavitt, B. R., Cullis, P. R., & van der Meel, R. (2021, June). The current landscape of nucleic acid therapeutics. *Nature Nanotechnology*, *16*(630–643), 1–14. https://www.nature.com/naturenanotechnology

22. Kumar, R., Santa Chalarca, C. F., Bockman, M. R., Bruggen, C. V., Grimme, C. J., Dalal, R. J., Hanson, M. G., Hexum, J. K., & Reineke, T. M. (2021). Polymeric

Delivery of Therapeutic Nucleic Acids. *Chemical reviews*, *121*(18), 11527–11652. https://doi.org/10.1021/acs.chemrev.0c00997

23. Lan, L., Guo, Q., Nie, H., Zhou, C., Cai, Q., Huang, J., & Meng, X. (2019). Linear-hairpin variable primer RT-qPCR for MicroRNA. *Chemical Science*, *10*(7), 2034–2043. https://doi.org/10.1039/c8sc04621b

24. Lee, J. S., Green, J. J., Love, K. T., Sunshine, J., Langer, R., & Anderson, D. G. (2009). Gold, Poly(β-amino ester) Nanoparticles for Small Interfering RNA Delivery. *Nano Letters*, *9*(6), 2402–2406. https://doi.org/10.1021/nl9009793

25. Liao, W. C., Lu, C. H., Hartmann, R., Wang, F., Sohn, Y. S., Parak, W. J., & Willner, I. (2015). Adenosine Triphosphate-Triggered Release of Macromolecular and Nanoparticle Loads from Aptamer/DNA-Cross-Linked Microcapsules. *ACS Nano*, *9*(9), 9078–9086. https://doi.org/10.1021/acsnano.5b03223

26. Lo RC (2013) Application of Microfluidics in Chemical Engineering. Chem Eng Process Tech 1: 1002.

27. Mansour, F. H., & Pestov, D. G. (2013). Separation of long RNA by agarose–formaldehyde gel electrophoresis. *Analytical Biochemistry*, *441*(1), 18–20. https://doi.org/10.1016/j.ab.2013.06.008

28. Masek, T., Vopalensky, V., Suchomelova, P., & Pospisek, M. (2005). Denaturing RNA electrophoresis in TAE agarose gels. *Analytical Biochemistry*, *336*(1), 46–50. https://doi.org/10.1016/j.ab.2004.09.010

29. Mejía-Salazar, J. R., Rodrigues Cruz, K., Materón Vásques, E. M., & Novais De Oliveira Jr., O. (2020). Microfluidic Point-of-Care Devices: New Trends and Future Prospects for eHealth Diagnostics. *Sensors*, *20*(7), 1951. https://doi.org/10.3390/s20071951

30. Padhi, B. K., Singh, M., Rosales, M., Pelletier, G., & Cakmak, S. (2018). A PCR-based quantitative assay for the evaluation of mRNA integrity in rat samples. *Biomolecular Detection and Quantification*, *15*, 18–23. https://doi.org/10.1016/j.bdq.2018.02.001

31. Palamà, I. E., Cortese, B., D'Amone, S., & Gigli, G. (2015). mRNA delivery using non-viral PCL nanoparticles. *Biomaterials Science*, *3*(1), 144–151. https://doi.org/10.1039/c4bm00242c

32. Park, K. S., Sun, X., Aikins, M. E., & Moon, J. J. (2021). Non-viral COVID-19 vaccine delivery systems. *Advanced Drug Delivery Reviews*, *169*, 137–151. https://doi.org/10.1016/j.addr.2020.12.008

33. Picó, Y. (2007). *Food Toxicants Analysis: Techniques, Strategies and Developments* (1st ed.). Elsevier Science.

34. SPOHR, G., MIRAULT, M. E., IMAIZUMI, T., & SCHERRER, K. (1976). Molecular-Weight Determination of Animal-Cell RNA by Electrophoresis in Formamide under Fully Denaturing Conditions on Exponential Polyacrylamide Gels. *European Journal of Biochemistry*, *62*(2), 313–322. https://doi.org/10.1111/j.1432-1033.1976.tb10163.x

35. Sridharan, K., & Gogtay, N. J. (2016). Therapeutic nucleic acids: current clinical status. *British Journal of Clinical Pharmacology*, *82*(3), 659–672. https://doi.org/10.1111/bcp.12987

36. St. Clair, N., Shenoy, B., Jacob, L. D., & Margolin, A. L. (1999). Cross-linked protein crystals for vaccine delivery. *Proceedings of the National Academy of Sciences*, *96*(17), 9469–9474. https://doi.org/10.1073/pnas.96.17.9469

37. Sultana, A., Zare, M., Thomas, V., Kumar, T. S., & Ramakrishna, S. (2022). Nano-based drug delivery systems: Conventional drug delivery routes, recent developments and future prospects. *Medicine in Drug Discovery*, *15*, 100134. https://doi.org/10.1016/j.medidd.2022.100134

38. Tolochko, N. K. (2008). HISTORY OF NANOTECHNOLOGY. *Encyclopedia of Life Support Systems (EOLSS)*, 1–6.

39. Ueno, T. (2013). ChemInform Abstract: Porous Protein Crystals as Reaction Vessels. *ChemInform*, *44*(42), no. https://doi.org/10.1002/chin.201342260

40. Wang, D., Stuart, J. D., Jones, A. A., Snow, C. D., & Kipper, M. J. (2021). Measuring interactions of DNA with nanoporous protein crystals by atomic force microscopy. *Nanoscale*, *13*(24), 10871–10881. https://doi.org/10.1039/d1nr01703a

41. Widdel, F. (2007). Theory and Measurement of Bacterial Growth. *Grundpraktikum Mikrobiologie*.

42. Yan, E. K., Cao, H. L., Zhang, C. Y., Lu, Q. Q., Ye, Y. J., He, J., Huang, L. J., & Yin, D. C. (2015). Cross-linked protein crystals by glutaraldehyde and their applications. *RSC Advances*, *5*(33), 26163–26174. https://doi.org/10.1039/c5ra01722j

43. Yu, R. C., Hanson, P. I., Jahn, R., & Brünger, A. T. (1998). Structure of the ATP-dependent oligomerization domain of N-ethylmaleimidesensitive factor complexed with ATP. *Nature Structural Biology*, *5*(10), 924. https://doi.org/10.1038/2368

44. Zimmerman, J.J., Arnim, A.V., & McLaughlin, J. (2011). Chapter 74 – Cellular Respiration.